12-2016

Uncertainty quantification on industrial high pressure die casting process

Jiahong Fu
Purdue University

Follow this and additional works at: https://docs.lib.purdue.edu/open_access_theses

Part of the Mechanical Engineering Commons

PURDUE UNIVERSITY
GRADUATE SCHOOL
Thesis/Dissertation Acceptance

This is to certify that the thesis/dissertation prepared

By Jiahong Fu

Entitled
UNCERTAINTY QUANTIFICATION ON INDUSTRIAL HIGH PRESSURE DIE CASTING PROCESS

For the degree of   Master of Science in Mechanical Engineering

Is approved by the final examining committee:

Amy M. Marconnet
Co-chair

Matthew J. Krane
Co-chair

Ilias Bilionis

To the best of my knowledge and as understood by the student in the Thesis/Dissertation
Agreement, Publication Delay, and Certification Disclaimer (Graduate School Form 32),
this thesis/dissertation adheres to the provisions of Purdue University's "Policy of
Integrity in Research" and the use of copyright material.

Approved by Major Professor(s):   Amy M. Marconnet

Approved by: Jay P. Gore   12/5/2016

Head of the Departmental Graduate Program   Date

UNCERTAINTY QUANTIFICATION ON INDUSTRIAL HIGH PRESSURE DIE

CASTING PROCESS

A Thesis

Submitted to the Faculty

of

Purdue University

by

Jiahong Fu

In Partial Fulfillment of the

Requirements for the Degree

of

Master of Science in Mechanical Engineering

December 2016

Purdue University

West Lafayette, Indiana

For my parents

Zehang Fu and Xiaoling Cai

ACKNOWLEDGEMENTS

TABLE OF CONTENTS

LIST OF TABLES

LIST OF FIGURES

ABSTRACT

Jiahong, Fu. M.S.M.E., Purdue University, December 2016. Uncertainty Quantification on Industrial High Pressure Die Casting Process. Major Professor: Amy Marconnet, School of Mechanical Engineering and Matthew Krane, School of Materials Engineering.

High pressure die casting (HPDC) is a famous manufacturing technology in industry. This manufacturing process is simulated by commercial code to shed the light on the quality of casting product. The casting product quality might be affected by the uncertainty in the simulation parameter settings. Thus, the uncertainty quantification on HPDC process is significant to improve the casting quality and the manufacturing efficiency.

In this work, three uncertainty quantifications and sensitivity analyses on the A380 aluminum alloy HPDC process of intermediate speed plate are performed. The material thermophysical properties, boundary conditions of the model, and operational as well as artificial parameters with their uncertainties, are considered as the inputs of interest. Uncertainty quantification and sensitivity analyses are investigated for the outputs of interest including percent volume of porosity result, percent volume of fraction solid less than 1, and the percent volume that solidified during multiple solidification times. The most influential input parameter for predicting the outputs of interest is the boundary condition of metal-die interfacial air gap.

CHAPTER 1. INTRODUCTION

1.1   Introduction

The earliest examples of die casting by pressure injection, as opposed to casting by

gravity alone, dates back to the mid-1800s [1]. The die casting process evolved from low-

pressure injection casting method to the techniques including High Pressure Die Casting

(HPDC), Squeeze Casting, and Semi-solid Die Casting. Compared to other casting

processes, such as sand casting and plastic molding casting, die casting can not only

shorten the manufacturing cycle time but also produce the complex components and

thinner-wall structures with better stability and durability. Die casting, especially of

aluminum, is widely used in the automotive industry for high-volume productions such as

engine blocks and cylinder heads. The selection of aluminum alloy in HPDC is due to

their favorable combination of low weight, easy machinability, and low cost [2, 3].

In HPDC processes, the molten metal flows into a metallic mold under very high

pressure (100+ bar) [4]. Then, this high pressure is maintained during the solidification

process, also called intensification, until the die is opened and the casting is ejected. Such

external high pressure improves the feeding ability of the liquid, ensuring that every

regions in the die cavity is filled successfully, and reduce the pores or voids in the

resulting part. Based on differences in the filling process, HPDC can be categorized as

Cold Chamber Die Casting (CCDC) or Hot Chamber Die Casting (HCDC), both of which

are displayed in Figure 1.1. CDCC process requires a ladle controlled by the machine arm

to scoop the molten metal out of the furnace and then pour it into the shot cylinder. After

the plunger pushes the liquid metal into the die cavity, which is called filling process, the

solidification begins. In contrast, HCDC does not require ladle to finish the filling

process. The shot cylinder in the HCDC process is partly immersed inside the molten

metal pot and during the filling process, the plunger pushes the molten metal from inside

the molten metal pot towards the die cavity. HCDC is advantageous, compared to CDCC,

for die casting of low melting-temperature alloys since the liquid metal will not suffer

from the pre-crystallization (that might happen in the shot cylinder in CDCC).

(a)   (b)
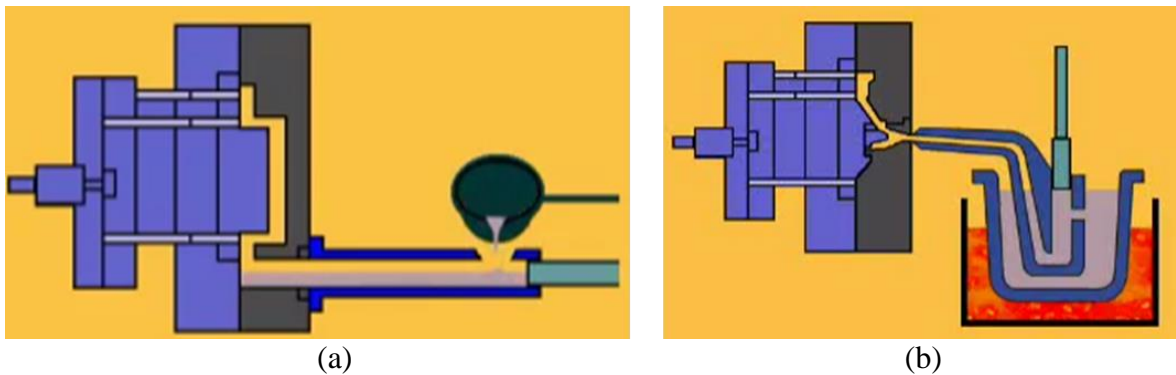
Figure 1.1. High Pressure Die Casting Schematics. In (a) cold-chamber die casting, the shot cylinder is placed outside the molten metal pot, whereas in (b) hot-chamber die casting, the shot cylinder is partially immersed in the molten metal during the filling process. Images reproduced with permission from [1].

In addition to the casting solidification process, there are several preparation steps in the

casting process required before the filling process begins, most importantly, spraying and

blowing. Spraying lubricates the surface of die cavity in order to prevent the soldering

reaction that leads to wear of the die surface and damage of the casting part. However, because of the high temperature at the die surface in the production cycle, the water-chemical mixed lubricant evaporates before it reaches the surface. Thus, the subsequent blowing step works as an 'air fan' to blow lubricant towards the die cavity surface efficiently, ensuring that the lubricant particles attach to cavity surface before the filling of liquid metal.
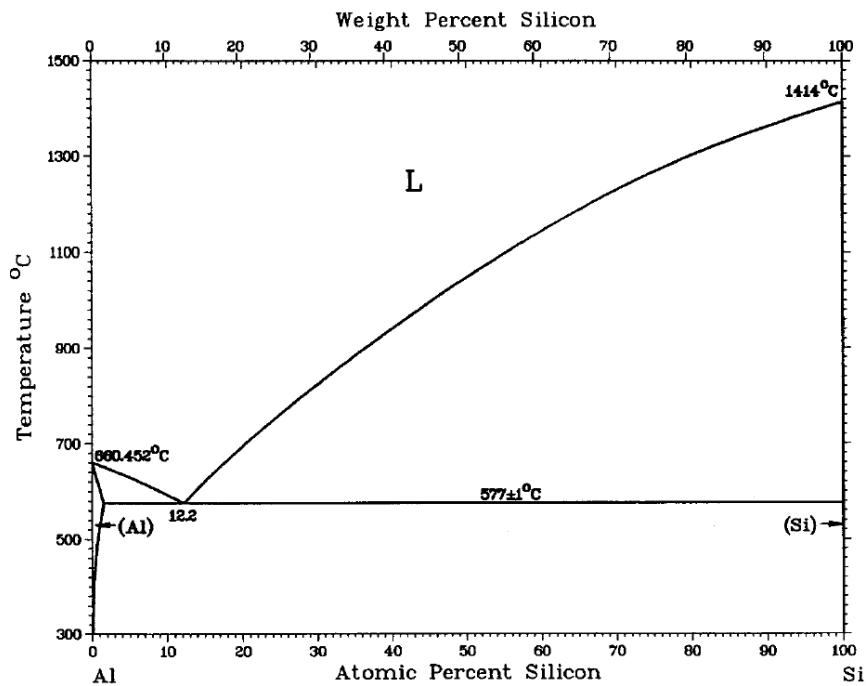
Figure 1.2. Al-Si Binary Phase Diagram. Aluminum A380 contains XX% Si and thus the liquidus temperature is ~XX and solidus temperature is ~XX. Reproduced with permission from [5].

Aluminum alloys are widely used in the HPDC process, especially those in the Al-Si alloy family. Silicon decreases the thermal expansion coefficient, while increasing corrosion and wear resistance for the Al-Si alloy [5]. The most common alloys in automobile industry are Al-9Si-3Cu (A380) and Al-17Si-4.5Cu (A390), both of which are used in the casting of transmission housing, engine block, and cylinder head because

of the great fluidity and castability of the alloy. According to the Al-Si binary phase diagram, Figure 1.2, it is a eutectic system with the eutectic composition at 12.2 wt. % Si [5]. Thus, A380 is hypoeutectic and A390 is hypereutectic one.

When the Al-Si alloy solidifies, the primary phase, α-Al, forms as the matrix and grows in dendrites [5]. The silicon phase forms and grows in angular primary particles. According to the Al-Si binary phase diagram, Figure 1.2, it is a eutectic system with the eutectic composition at 12.2 wt. % Si [5]. Thus, A380 is hypoeutectic and A390 is hypereutectic. At the eutectic point, 12.2 wt. % Si, the eutectic phases form and grow during the solidification. The hypoeutectic alloy, A380, has the soft and ductile α-Al phase as primary matrix and the hard but brittle eutectic silicon phase β (α-Al + Si) in the interdendritic regions. The hypereutectic alloy, A390, contains coarse and angular silicon particles and eutectic silicon phase β.

Other elements included in Al-Si alloys such as copper (Cu), magnesium (Mg), Manganese (Mn), also impact the performance of casting. Copper strengthens these alloys through the precipitation of secondary eutectic phases of $CuAl_2$ intermetallic [2]. Mg also increases the strength of alloy and its corrosion resistance. Mn is introduced in this alloy mainly to compensate the negative effect of iron (Fe) impurities [3]. The Fe-based precipitates are acicular structures in the Al-Si alloy. This type of morphology is deleterious to the material performance since the sharp precipitates are ideal places for stress concentration leading to the micro-crack propagation under the external loading. With the introduction of Mn, a Fe-Mn intermetallic is formed that transforms the Fe-based acicular type structure into a more complex shape [2] that can improve the elongation property of Al-Si alloys.

Castings often have defects including inclusions and porosity. Inclusions come from the oxide and silicate usually unintentionally picked up during the melting and the feeding process [5]. These defects are the weakest positions in the microstructure and easily lead to stress concentration and failure.

Porosity can be categorized as two types: shrinkage porosity and gas porosity. In HPDC, shrinkage pores result from the density difference between the liquid phase and solid phase of alloy. Porosity is also controlled by the solidification process [5, 6]. During the solidification, the temperature range between liquid and solidus temperature of alloy is called freezing range. In this range, dendrite structures form first and interact with each other, leading to the interdendritic regions in which the Al-Si eutectic phases form at the end of solidification. The interaction of dendrite structures at a critical fraction solid prevents the filling of additional liquid metal from such interdendritic regions. Therefore, the density change from liquid phase to solid phase of Al-Si eutectics leads to shrinkage pores. Based on the fraction solid at which the interaction of dendrites really stops the filling, the freezing range has been further manually classified as two zones—the slurry zone and the mushy zone. In the slurry zone, the liquid metal flows, driven by the buoyance force [7] or the external pressure. Thus, the shrinkage pore formed inside the slurry zone can still be filled by the liquid metal flow. However, in the mushy zone, since the fraction solid has reached the critical value, the rest of the liquid metal in the interdendritic regions will change phase with the formation of shrinkage pores in regions blocked. In HPDC, during the intensification process, the external high pressure drives the liquid metals flow to overcome the interdendritic arm barrier and feeds the shrinkage

pores in the interdendritic regions. Thus, HPDC reduces the level of shrinkage porosity to some extent compared to lower pressure casting methods.

(a)   (b)
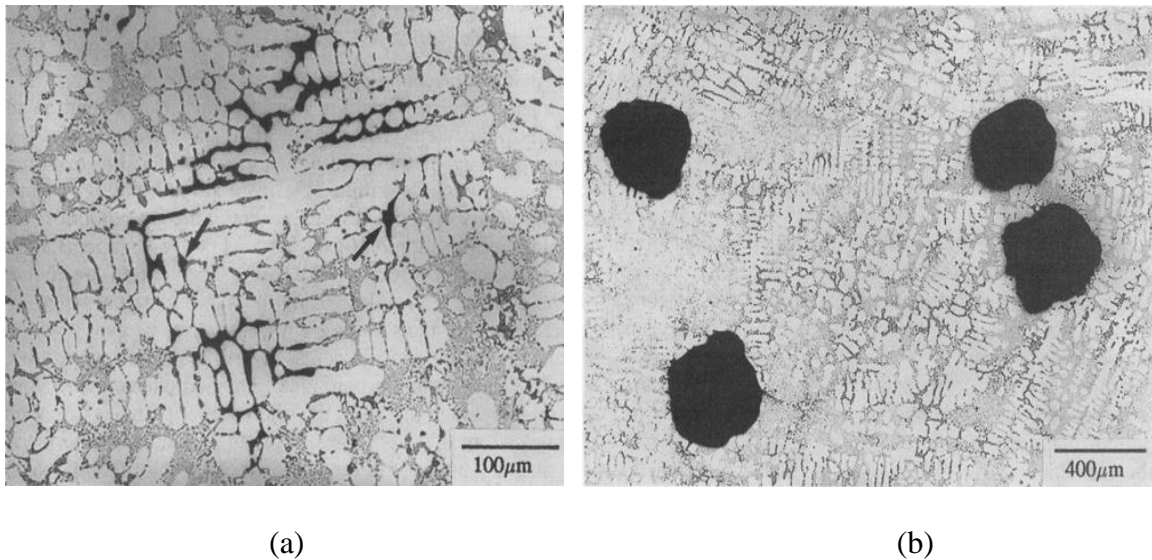
Figure 1.3. (a) Shrinkage Pores (b) Gas Pores. Reproduced from [8].

Compared to shrinkage porosity, gas porosity is often more deleterious. The size of gas pores are larger than shrinkage pores located in the interdendritic regions, as shown in Figure 1.3 [8] . Undoubtedly, if gas pores are not avoided in HPDC process, it often leads to disastrous failure of the part. Gas porosity can be categorized into two types—air entrapments and hydrogen gas pores. Air entrapment comes from the failure of the drainage of air originally inside the die cavity during the filling process. Optimization of the venting system in the mold and casting part geometry can minimize the air entrapment. Hydrogen gas pores are generated and grow during solidification process with the exsolution of the hydrogen content. The solution of hydrogen in Al-Si melt increases as temperature increases. Thus, during the solidification process, hydrogen atoms precipitate from the melt and form molecular hydrogen [5]. When the local

hydrogen gas pressure exceeded the critical pressure, the hydrogen gas pore forms. Such

formation can be described by the relation $\Delta P = 2\sigma/r$, where σ is the surface tension and

ΔP is the critical pressure that must be exceeded for a pore nucleation with critical radius

r to grow [8]. With the nucleus of a pore, hydrogen atoms from other region will move

forward to this pore by mass diffusion and then the pore grows. The fast solidification

process from HPDC can efficiently suppress such hydrogen diffusion because of its short

solidification time. In such fast phase transformations, the hydrogen is not able to

precipitate enough hydrogen atoms to form a gas pore. Thus, heat treatment does not

improve the mechanical properties of HPDC parts, because such a process will instead

lead to the re-growing of the hydrogen gas pore, also called a blister [1].

1.2   Process Modeling & Uncertainty Quantification for Die Casting

The solidification process in casting is complex. In order to describe the associated

physical phenomenon, numerical models of alloy solidification have been developed and

used to predict the transport phenomena and solidification. Wang and Beckermann [9,

10] applied a multiphase model in which each phase has its own unique conservative

equation. Vreeman et al. [11-13] applied the continuum mixture method, in which the

transport equations function for each phases were written in terms of the mixture of all

phases included. This method was developed and applied specifically for the steady state

direct chill casting simulation of Al alloys, and recently extended to the simulation of

transient direct chill casting process [14]. Since it is impossible to obtain every physical

detail in laboratory experiments, numerical simulations can provide tremendous insight

into the transport phenomena happening in the casting process. However, the predictions

from models are typically reported with arbitrary precision without consideration of the uncertainties inherent in the choice of models, the values of material properties, or boundary conditions. The lack of understanding of uncertainty propagation in the solidification process limits the effective application of such models to predictions for industrial casting process. Determining the source of possible uncertainties, and then understanding and quantifying their effect on the final prediction allows for better estimation of the margins of safety and improves process reliability.

Fezi and Krane [15, 16] have successfully applied the uncertainty quantification in their works on numerical modeling of metal solidification, beginning to answers questions about which input parameters have the great influence on the outputs of interest and identifying key experimental priorities to improve the accuracy of solidification models. The methodology of the uncertainty quantification is also described in detail in their works, including the categorization of the uncertainties, sensitivity analysis process, and a computational tool for uncertainty quantification.

There are two kinds of model uncertainties in solidification models—epistemic and aleatoric [17]. Epistemic uncertainty comes from a limited knowledge about the system being simulated, for example, an inaccurate model selection in the numerical simulation. This uncertainty relates to uncertainty in the choice of models, for instance, the choice of permeability model [18, 19] and cannot be described by a probability function. The way to reduce epistemic uncertainty is to understand the physical phenomena better, so that the more accurate models can be made. The other type of uncertainty, aleatoric, arises from the inherent randomness of sampling data and the natural variation in measurements of various inputs such as material properties, geometric

parameters, etc. It can not be reduced without a better sampling method or data collection method in measurements. In casting solidification simulations, the uncertainties of material properties and boundary condition values from the experimental measurement belong to the class of aleatoric uncertainty. Based on the precision of the measuring facility, such aleatoric uncertainties can be represented by a probability distribution, such as a Gaussian distribution characterized by the mean value and normal standard deviation. In transient simulation processes, the uncertainty of process times during which the boundary condition are appropriate can also be considered as aleatoric in the uncertainty quantification process. The difference between the effect of epistemic and aleatoric uncertainty is displayed in the Figure 1.4 which shows that epistemic uncertainty is similar to the accuracy and describes the bias in the model, in comparison to that aleatoric uncertainty describes inherent randomness and the precision level [17].
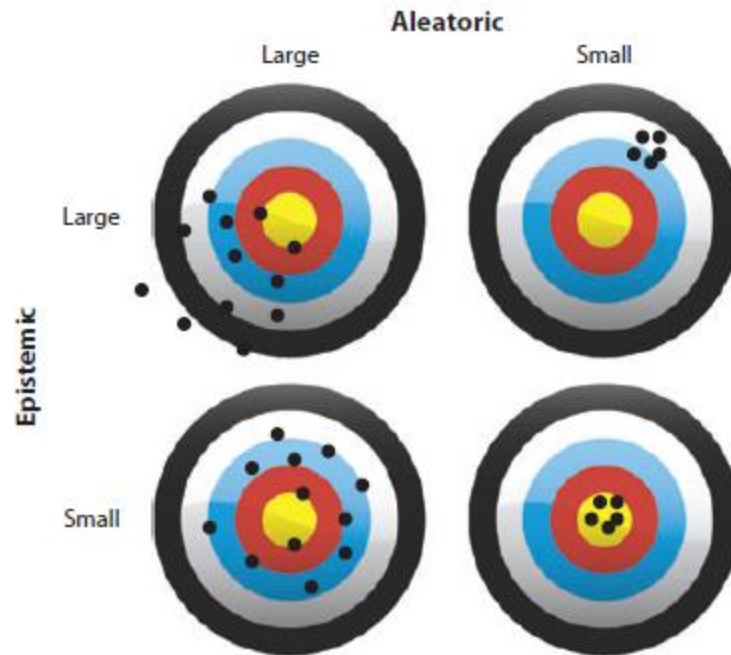
Figure 1.4. Effect of Aleatoic and Epistemic Uncertainties [17]. Closer to the yellow target represents the better predicted result. The aleatoric uncertainty controls the precision of the results while the epistemic determines the accuracy of the results.

In order to address aleatoric uncertainty, sensitivity analyses are often performed. The simplest method involves varying each of the input parameters individually over a range one at a time and then analyzing how the model responds to such variation. This method helps to understand how various input parameters affect the outputs of model but cannot provide information on the interactions of input parameters. For improved the quantification of aleatoric uncertainty considering these interaction, the most direct approach is a Monte Carlo Method [20], where a random combination of inputs are selected and the model is evaluated a large number of times in order to generate a probability density function (PDF) for each output quantity. This has proved to

be a very useful tool to estimate the probability of output values with uncertainties of inputs for the model. However, if the model is sophisticated and the computational time is long, such a Monte Carlo quantification approach is not efficient as it may require tens of thousands of evaluations of the numerical models to generate the final PDFs of outputs. One way to reduce this time and resource cost is to replace the real computational model with a surrogate model originating from a polynomial fitting based on a limited number of simulation results. This surrogate model is more computationally efficient than the real numerical model so the Monte Carlo quantification time is reduced significantly. Researchers in related fields have successfully constructed the surrogate model approach and used it to produce the PDFs of outputs in the uncertainty quantification of their computational models [21].

This thesis uses the PRISM Uncertainty Quantification (PUQ) framework to perform the uncertainty quantification. Detailed descriptions of this software can be found elsewhere [22], so here only a simple description will be provided. PUQ is a software package for the non-intrusive uncertainty propagation in through computer simulation codes and the associated analyses. It can also interact with commercial codes or software after further user development. Given the inputs of interest and known uncertainties, PUQ calculates PDF for each output of interest, for example, the time to solidification or temperature at a particular point in time and space. The outputs of interest are first sampled from the full numerical model to generate a polynomial response surface, which is the surrogate model that is used in the following process instead of the full numerical model. During the sampling process, the Smolyak sparse grid algorithm [23, 24] determines the sampling condition (number and values) of the

inputs of interest to generate the surrogate model. A level one Smolyak grid varies each

input with uncertainty independently and requires least number of sampling cases. It

generates a surrogate model that is linear for all inputs of interest since all the inputs are

assumed to lack of the interaction in the level one Smolyak sparse algorithm. Polynomial

chaos expansion (PCE) or global polynomial chaos (gPC) methods are applied in the

generation of surrogate model by fitting to those sparse model predictions from sampling

cases [24]. In a level one Smolyak grid sampling, only first order of polynomial fitting is

calculated. The level two and three Smolyak grid algorithms consider the interaction of

multiple inputs simultaneously and produce surrogate models with polynomial of second

and third order, respectively. With increasing level of the Smolyak algorithm, the number

of required sampling cases increases, thereby requiring more computational resources. As

an example, a level one Smolyak analysis needs $1+2n$ sampling cases to produce the first

order polynomial surrogate model, where n is the number of uncertainty inputs, but a

level 2 Smolyak analysis requires $1+4n+(4n(n-1))/2$ sampling cases to generate the

second order polynomial surrogate model. In practice, the choice of algorithm level needs

to be made by the users, considering tradeoff between the computational resource and the

accuracy of surrogate model.

The quality of the fit of the surrogate model to the sampling outputs from the full

numerical model is quantified with the Root Mean Square Error (RMSE). Low RMSE

means the surrogate model fits the sampling outputs well and it is reliable to use in place

of the original sophisticated numerical model in the following analyses. High RMSE

means the current order of polynomial is not able to fit the sampling outputs with

sufficient accuracy. In that case, a higher level of the Smolyak algorithm may be needed to produce better surrogate model.

The output PDF is calculated by using the Latin Hypercube sampling to evaluate response of the surrogate model over the input uncertainty range. The resulting PDF quantifies the probability of obtaining a particular output value, and is typically characterized by mean value and normal standard deviation. The integration of the PDF over all possible values should yield one unit. In industrial application, such integration can give information about the reliability of the process design. For example, this method can determine, the probability of the part is fully solid after 20 seconds of solidification process.

The relative sensitivities of the outputs to changes in the inputs are calculated by the Elementary Effects Method (EEM) [25]. The outputs from sampled cases are used by the EEM to determine the effect of the input on the outputs. The definition of elementary effect is given by

$$d(X_j) = EE_j = \frac{\Delta Y_j / \Delta X_j}{(X_{j,max} - X_{j,min})}, \tag{1}$$

where $(X_{j,max} - X_{j,min})$ is the sampling range of the inputs, ΔX_j is the (constant) step change for the sampled input, and ΔY_j is the difference of output to the changes of the input. Thus, a distribution of elementary effects is obtained for each input parameters.

In the PUQ framework, there are two sensitivity indicators being calculated. The mean, μ^*, of the distribution of absolute values of elementary effects is calculated by the equation: $\mu^* = \frac{1}{r}\sum_{j=1}^{r}|d(X_j)|$, in which r is the number of elementary effects considered

in distribution. The quantity of μ^* is used to determine to the level of effect of the input on the output. Greater values indicate that the input plays a more significant role in determining the output. Since the units of μ^* are the same as the output itself, this parameter shows the real impact of the input uncertainty on an output quantity. Another indicator of sensitivity, σ^*, is the standard deviation of all elementary effects in the distribution. A high value of σ^* means the impact of the particular input of interest is strongly affected by other inputs. Small values of σ^* show the influence of input is independent from other inputs and such inputs tend to have linear influence on output. In other words, quantity of σ^* indicates level of interaction of the inputs with each other or some non-linearity in the system. Thus, if only one input with the level one Smolyak sampling algorithm is considered in PUQ, the surrogate model will be a first order linear function, which is a crude assessment of the effect of input. But when the user cannot weigh the impact of inputs against each other, this level one uncertainty quantification (with a simple input) can give an insight of the impact of the input on outputs roughly by calculating the μ^*. No σ^* is computed in this case because of the lack of interaction with other inputs.

1.3   MAGMASOFT Introduction

MAGMASOFT is a commercial code that simulates the casting process for industrial application [26]. It provides a useful tool for the casting design engineers to optimize their casing and mold geometry without constructing the multiple prototypes experiments. It builds up a visible platform about the casting product between the design engineers and the manufacturing engineers.

Based on the difference fields of casting industry, the MAGMASOFT has been designed into various modules with different casting process. The prevalent modules include MAGMAiron for iron casting, MAGMAsteel for steel casting, MAGMAlpdc for low pressure die casting & non-ferrous casting, and MAGMAhpdc for high pressure die casting. This series of commercial codes provide a reliable tool for engineers to quality their casting products and quantify the potential defects in casting parts.

1.4   Uncertainty Quantification in MAGMAhpdc

In this work, uncertainty quantification is implemented in industrial HPDC process by using the PUQ framework. Instead of just considering the solidification process of casting, simulations of industrial HPDC process should include the multiple preparation steps before the liquid metal filling and solidification, such as spraying lubricate, blowing and operational delay, each of which has different heat transfer coefficient (HTC) curve as boundary condition for the mold. Simulations of HPDC process also consider the casting ejection step, which determines when the casting loses the contact with cover die and ejection die. These steps significantly change the casting-die interfacial heat transfer coefficient (IHTC) boundary condition and have a great impact on the casting results. Moreover, the thermal management of HPDC system is greatly controlled by the cooling channel system (CCM) installed in the dies. This CCM has great thermal influence on the dies temperature distribution and then even on the casting solidification process. Therefore, the HTC value and working time of CCM should also be focused on. The MAGMAhpdc module integrates all these HPDC process steps into its commercial code, providing industrial engineers with the powerful tool to analyze their HPDC production

process. Thus, this MAGMAhpdc module is selected as the object for the uncertainty

quantification through the PUQ framework. The MAGMAhpdc module belongs to

MAGMASOFT 5.2.

In order to quantify uncertainty in a real HPDC process, a model of real product

is applied in this work. Specifically, Fiat-Chrysler Automobiles (FCA) provided their

MAGMAhpdc model of intermediate speed plate, displayed in Figure 1.5, which is a part

of the transmission system in vehicle. The casting material is aluminum alloy A380 and

the die is made of H13 tool steel. The initial temperature of liquid A380 is set as 643.3℃.

The initial temperature of dies are set as 25 ℃ room temperature and several cycles of

casting are simulated to obtain realistic temperature distribution within the die before the

"production cycle" that is considered for the following uncertainty analysis. Considering

the limited computational resource and time, each simulation calculates the whole HPDC

process for just 10 cycles, including 9 cycles for pre-heating and, finally, 1 cycle for

production analysis. Heating cycles help the HPDC system to reach the quasi steady-state

thermal conditions, so that the following production cycles can produce stable high

quality casting products. Therefore, for each simulation, only the results from the last

(tenth) cycle are considered in the uncertainty quantification. The net heat flow into the

dies is an indication of whether the system has reached steady state conditions. The

Figure 1.6 shows 10-cycle simulation is enough for intermediate speed plate HPDC

system. The amount of net heat of the dies does not change significant after the eighth

casting cycle. That means the thermal conditions for the future HPDC cycles are similar

and the casting quality can be maintained in a stable level. Further, the simulation results

from MAGMASOFT proves the stable level of casting quality. The volume of porosity

results in ninth and tenth casting cycle are the same, and the difference of the volume of

the fraction liquid results at 20s between the ninth and tenth cycle is about 5%, which is

very small if comparing to the whole volume of the casting.
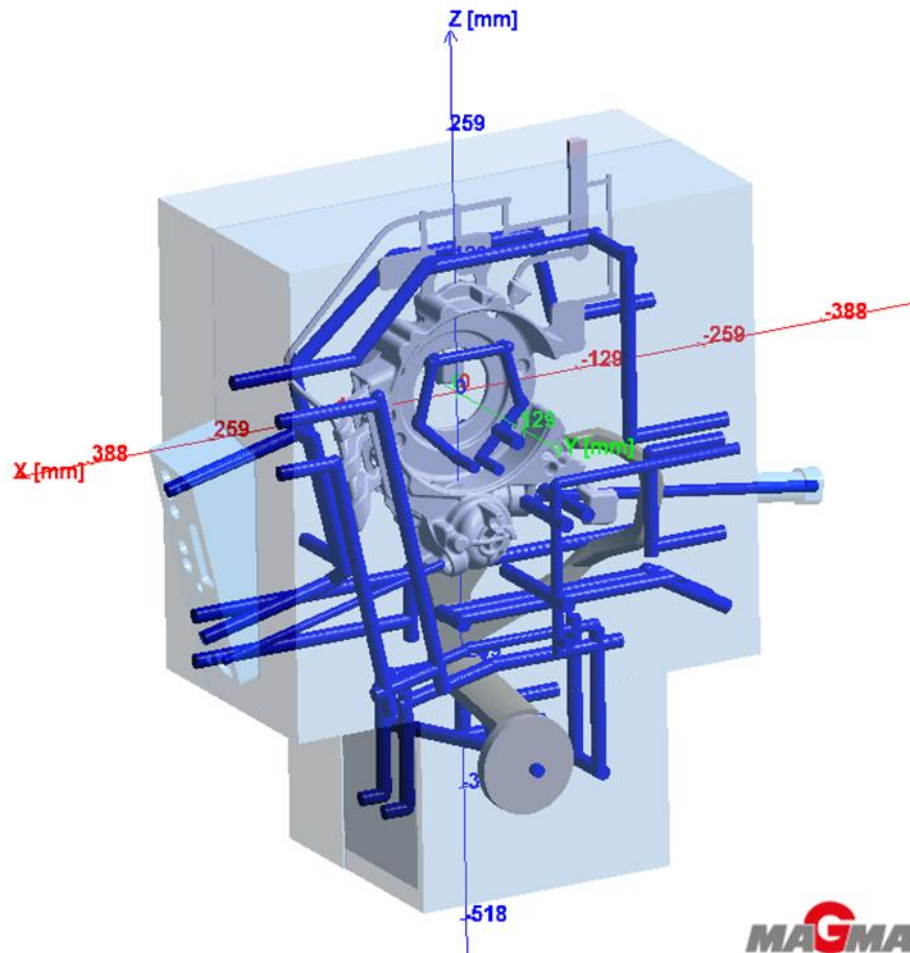
Figure 1.5. Model of Intermediate Speed Plate in MAGMASOFT. The transparent gray regions are the dies. The opaque gray part inside the dies is the casting (including the product, overflow, runner and biscuit). The blue channels around the casting are the cooling lines. The liquid metal is injected into the cavity from the biscuit.
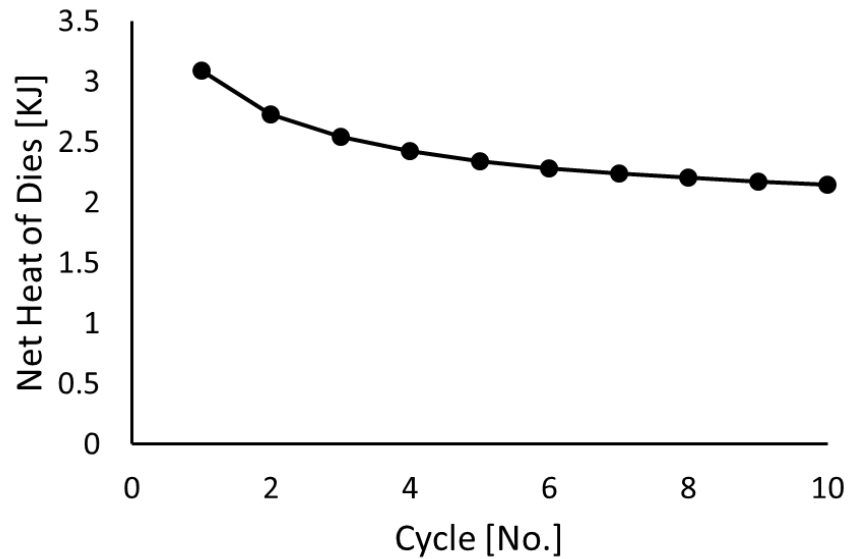
Figure 1.6. Heat balance for the dies. The black dots indicates the net heat transferred into the dies during each cycle. The heat balance becomes relatively constant with increasing cycling, which is a criterion to judge whether the HPDC system has reached the quasi steady-state thermal condition.

Three series of uncertainty quantification are conducted in this work. First, the impact of uncertainty in thermophysical properties of casting material is evaluated, aiming to quantify the effect of material properties uncertainties on casting results. This study sheds the light on the casting performance of this type of material in certain geometry. Second, the impact of uncertainty in several of the boundary conditions, is studied, in order to evaluate which boundary condition has the great impact on the final results. This study identifies which HTC curves should be measured with more accuracy in order to improve the simulation accuracy greatly. Third, uncertainty in feeding effectivity, spraying and the key interfacial heat transfer coefficient (IHTC) between the die and the casting are considered. Feeding effectivity in MAGMASOFT is a solidification model pre-set value determining at which fraction solid the surrounding

liquid metal stops filling the local position. This parameter obviously influences the casting defects (porosity). The spraying step aims to cover the lubricant in the surface of die to reduce the possibility of soldering. But it might change the initial temperature field in the surface of die before the metal filling process, leading to the changes in the casting results. Therefore, the third uncertainty quantification compares the effect of model settings, step setting and boundary conditions on the HPDC process. The uncertainty quantification investigations in this work are only restricted in the specific casting product(geometry), specific casting material and specific HPDC process parameters setting. All the HPDC simulations are done in MAGMASOFT 5.2 version. Any new functions belongs to the following MAGMASOFT version 5.3 are not used and discussed in this work.

CHAPTER 2. UNCERTAINTY QUANTIFICATION ON THERMOPHYSICAL PROPERTIES OF CASTING MATERIAL IN HPDC

2.1   Introduction of Experiments

Based on the uncertainty quantification results for the solidification models of Krane and colleagues [15, 16, 27, 28], thermophysical parameters (thermal conductivity (k), heat capacity (C_p), and the density (ρ) changes from liquidus to solidus) play a very important role in macrosegregation level models of aluminum direct chill casting [27]. Additionally, recent results illustrate that the latent heat (L_f) exerts the greatest influence on the macrosegregation for equiaxed alloy solidification [16]. Such uncertainty quantification results demonstrate that the effects of material properties vary depending on the solidification process. Thus, each solidification model must be carefully investigated independently. Moreover, no uncertainty quantification analysis has been done on the HPDC process and the effects of the thermophysical properties of casting material on the casting results are still unknown. Therefore, it is necessary to conduct the uncertainty quantification on thermophysical properties of casting material experiments. John Coleman is acknowledged for the collection of all material properties for this portion of the uncertainty quantification investigation.

2.2   Input of Interests

The alloy of particular interest in industrial HPDC is aluminum alloy A380. In this uncertainty quantification investigations, thermal conductivity (k), heat capacity (C_p), density (ρ) and latent heat (L_f) are considered as inputs of interest. Values of these material properties as a function of temperature in the default MAGMASOFT database comes from experiments, and from JMatPro, a computational software based on thermodynamic principles. To ensure the accuracy of the HPDC simulation, material properties extracted directly from experiments with the associated measurement uncertainty would be ideal for this uncertainty quantification. However, to the best knowledge of the author, no direct investigation on the thermophysical properties of A380 at the high temperature range of HPDC yet exists. Rather, the data for the thermal conductivity of A380 as a function of temperature, see Figure 2.1 (a), is obtained from the electrical resistivity measurement of Al-9Si-3Cu ternary alloy, with a maximum of 6% uncertainty displayed as the error bar [29].

Although without the related experimental data of other properties of A380, the thermophysical properties of A319, whose compositions are similar to A380, are found from the database. Compositions of both alloys are displayed in Table 2.1 [1, 30]. The nominal compositions of silicon and copper of A380 are 8.5% and 3.5% respectively. The key difference between A380 and A319 is the silicon content: A380 contains roughly 2% more than the A319 alloy. Due to the similarity of their compositions, the high temperature experimental properties of A319, with the associated measurement uncertainties, are assumed to for the A380 in this uncertainty quantification of casting material properties.

Table 2.1. Alloying Components (wt.%) of A319 and A380 [1, 30].

Component	A319	A380.0
Si	6.1	7.50-9.50
Cu	3.01	3.00-4.00
Zn	0.71	<3.00
Fe	0.68	<1.30
Mn	0.32	<0.50
Sn	--	<0.35
Mg	--	<0.10

The apparent heat capacity of A319, see Figure 2.1 (b), is measured by differential scanning calorimetry (DSC) [30]. The uncertainty in DSC measurements is typically reported in the range of 3-5% [31]. In this uncertainty quantification investigation, 5% measurement uncertainty has been applied across the entire range of temperatures and is displayed as the error bar in Figure 2.1 (b). The effect of Si on heat capacity of aluminum alloys cannot be estimated from open literature, but is expected to be relatively small.

(a)

(b)
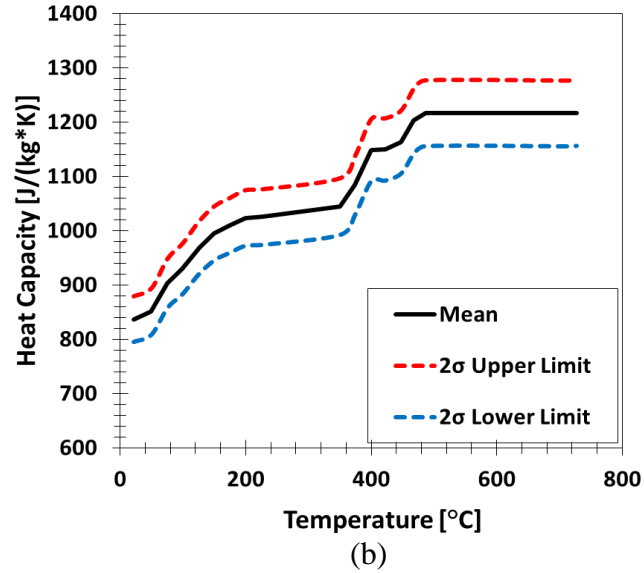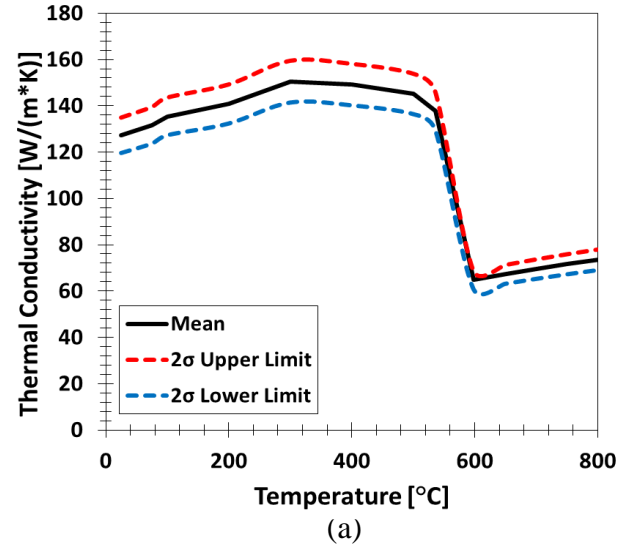
Figure 2.1 (a) Thermal Conductivity of A380 (b) Heat Capacity of A319. Black line indicates the experimental data from measurement. Two dash lines indicate their extreme experimental uncertainty—6% for thermal conductivity and 5% for heat capacity—as 2σ away from the black curve, representing a Gaussian distribution of uncertainty.
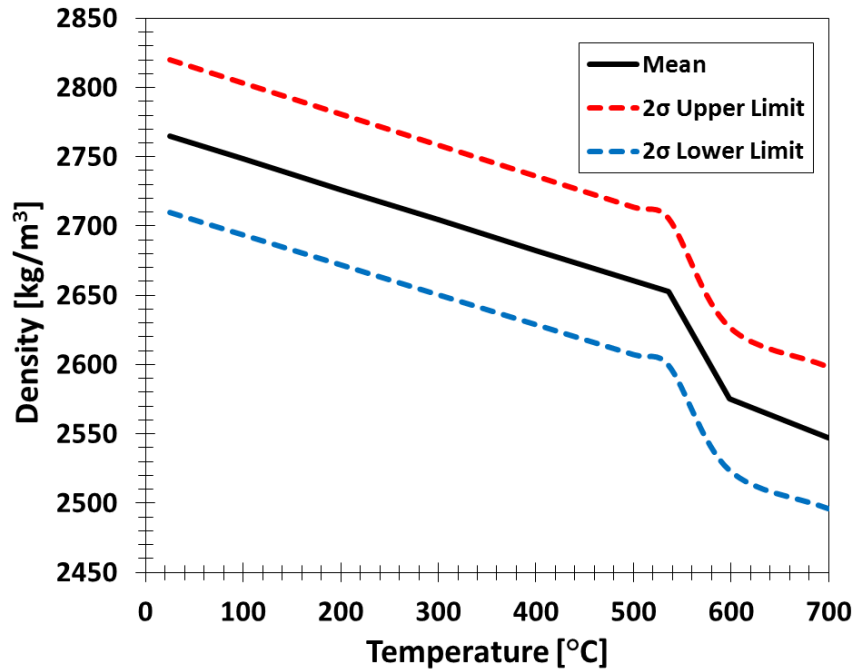
Figure 2.2. Density of A380. Black line indicates the data summarized from the literature. Two dash lines indicate the extreme experimental uncertainty, 2%, as 2σ away from the black curve, representing a Gaussian distribution of uncertainty.

The density of A380, or Al-9Si-3Cu, at room temperature is 2765 kg/m^3 [29]. However, the density curve as a function of temperature, especially under high temperature, is largely unknown. In order to estimate the density at high temperature, the slope of the density curve of A319 [30] is obtained and applied to the A380 density as a function of temperature. Figure 2.2 shows the predicted density curve for A380 with an uncertainty of 2% from the push-rod dilatometer modified for both solid and liquid metals density measurement of A319 [32].

The latent heat of A380 is calculated by Si Equivalency method [33, 34]. The accuracy of this method has been verified by the comparison with experimental data form DSC measurement. First, such method establishes silicon equivalent, Si_{EQ}, algorithm

which summarizes the effect of all alloy elements present in the Al-Si alloy in terms of a simple value of Si_{EQ}. Thus, the A380 alloy is assumed as a binary $Al\text{-}Si_{EQ}$ alloy in such case and the binary Al-Si phase diagram can be applied with the use of Lever Rule or Scheil's equation to calculate the amount of primary α-Al, $f_{Primary}^{\alpha-Al}$, and eutectic phase of Al-Si which can be divided into secondary Al, $f_{Secondary}^{Al}$, and Si fraction, $f_{Eutectic}^{Si}$, respectively. By knowing the value of latent heat of the solidification for pure aluminum, L_{f-Al} (190 kJ/kg) and pure silicon L_{f-Si} (1800 kJ/kg), the total latent heat of A380 can be calculated by:

$$L_f = f_{Primary}^{\alpha-Al} * L_{f-Al} + f_{Secondary}^{Al} * L_{f-Al} + f_{Eutectic}^{Si} * L_{f-Si} \qquad (2)$$

For A380, the latent heat is 496 kJ/kg, with 2.5% uncertainty coming from the real Si composition range of A380, from 7.5-9.5 wt. %.

Four thermophysical properties (k, C_p, ρ and L_f) with their uncertainties are submitted as inputs of interest to the PUQ framework which generates the required sampling cases for the generation of the surrogate model, and subsequently, the output PDFs calculation. Since k, C_p and ρ are temperature dependent, they are normalized first so that they can be submitted to PUQ framework as a simple value. In other words, $k_{PUQ}(T) = N * k_{exp}(T)$ such that the single parameter N can be varied to shift the curve. Their uncertainties are all considered to be Gaussian distributions since they come from the derivation of experimental measurement or composition variation with confidence in accuracy. Thus, the deviations (σ) of the Gaussian distribution submitted to the PUQ framework should be half of the uncertainty value of properties respectively, representing 95% confidence in the accuracy. In this uncertainty quantification, only the aleatoric

uncertainty from the experimental measure is considered, and the epistemic uncertainty

from the experimental methodology is neglected. All of these inputs of interest for PUQ

are summarized in Table 2.2 Considering the potential interaction of these four

parameters in HPDC process simulation in MAGMASOFT, a level 2 Smolyak algorithm

is applied in this uncertainty quantification, generating 41 sampling cases, each of which

has its own input parameters as MAGMASOFT simulation setting. After computing these

41 simulation cases, outputs of interest are accumulated and submitted to the PUQ

framework to obtain the surrogate model and output PDFs.

Table 2.2. Inputs of Interest for Uncertainty Quantification on Material Properties.

Property	Normalized Mean(μ)	2σ
Density	1	2%μ
		0.02
Thermal Conductivity	1	6%μ
		0.06
Heat Capacity	1	5%μ
		0.05
Latent Heat	1	2.5%μ
		0.025

2.3 Outputs of Interest

In this uncertainty quantification of material properties, the percent volume of porosity,

the fraction of liquid remaining at multiple solidification times are considered as the

output of interest. The first parameter represents the potential volume that might have

shrinkage pores in casting. This result is a major indicator of casting quality since the pores in casting will result in stress concentration, a cause for cracking in performance. Lower percent volume of porosity indicates good casting quality. The second parameter is the fraction liquid remaining at multiple solidification times, which shows the solidification sequence of casting. The usage of fraction liquid as an output of interest is to determine the reliability of the casting ejection time. When a sufficient fraction of the part is solidified, the casting can be ejected. Thus, this parameter helps to determine if the casting time can be reduced so that the manufacturing capacity is improved.

2.4   Results and Analysis

2.4.1   Porosity

A typical HPDC simulation porosity result from MAGMASOFT is shown in the Figure 2.3. The blue packages illustrated within the casting are the potential volumes in which the shrinkage pores might form. Thus, the volumes of blue packages are calculated for every simulation cases as the porosity volume for the uncertainty analysis.
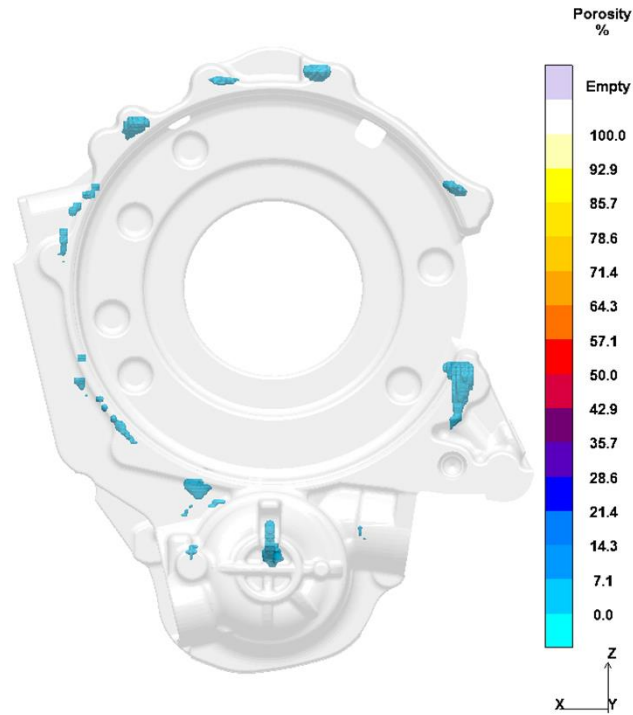
Figure 2.3.   Predicted porosity result from MAGMASOFT. The blue packages indicate the possible volumes in which the shrinkage pores form.

Figure 2.4 gives the sensitivity of the predicted porosity volume to the uncertain material properties. The thermal conductivity k has the greatest effect on the predicted porosity result. Since k is an indicator of speed of heat transfer, it determines the occurrence and completion time of solidification process. Based on the mechanism of pore formation discussed in Chapter 1, longer solidification time helps the liquid metal to feed the shrinkage pore with the assistance of external high pressure. Thus, the uncertainty of k actually leads to the uncertainty of casting solidification time and further to the uncertainty in the predicted porosity at the end of casting. Two properties, the latent heat L_h and density ρ, have similar elementary effects on the predicted porosity. Both of them have a larger impact on the porosity than the heat capacity C_p. The Stefan

number, $\left(C_p\Delta T_m \big/ L_h\right)$ for this A380 casting material, is about 0.15, which means L_h

dominates the solidification time, rather than sensible heating and the heat capacity.

Therefore, due to the linkage between solidification time and shrinkage pores, it is

reasonable to conclude that the influence of L_h on predicted porosity is larger than that of

C_p. The density, with the function of temperature indicative of the shrinkage tendency in

solidification, undoubtedly has an effect on the shrinkage pore formation as overall

volume reduced depends on the difference in density between the solid and liquid states.

However, its effect is not as important as the effect of k in this case. When comparing the

means (μ) of elementary effects (represented by the heights of histogram in Figure 2.4),

all material parameters significantly impact the porosity in this experiment. All of their

influences contribute to the final predicted porosity volume result. The long error bars on

the sensitivity indicate that these four material properties have non-linear combined

effects on the predicted porosity results. Thus, the interaction of material properties in the

MAGMASOFT porosity calculation model is strong.
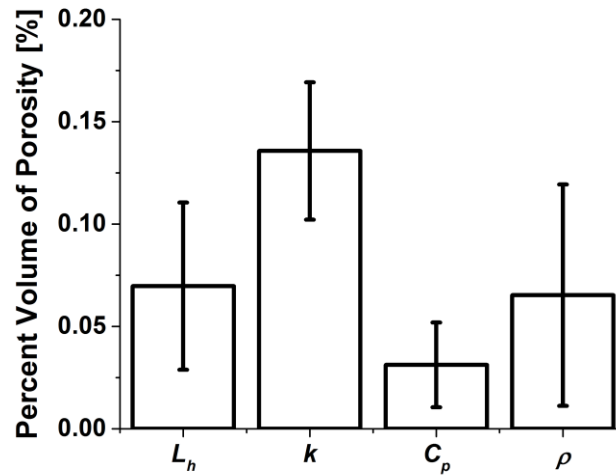
Figure 2.4. Elementary effect of material properties on the porosity result. The height of the histograms of L_h, k, C_p and ρ represent the mean (μ) of elementary effect over the uncertain range of latent heat, heat conductivity, heat capacity and density, respectively. The error bars for each histogram indicates magnitude of the interaction on the porosity result between material properties.

The resultant PDF calculated from level 2 quadratic polynomial surrogate model for predicted porosity is shown in Figure 2.5. The RMSE of the surrogate model is 15%. The PDF describing the model uncertainty is approximately a Gaussian distribution with a mean (μ) of 1.01% and a deviation (σ) of 0.03%, which constitutes an uncertainty $(^{2\sigma}/_\mu)$ of 5.9% for the predicted porosity. This very small uncertainty in the output porosity demonstrates that the uncertainty in thermophysical properties of A380 ultimately has very little impact on the predicted porosity volume. This is not surprising since the solidification time of HPDC process is sufficiently short that other parameters, which directly control the solidification rate like boundary conditions, might have more

severe effect on the formation of shrinkage pores during the short time solidification process.
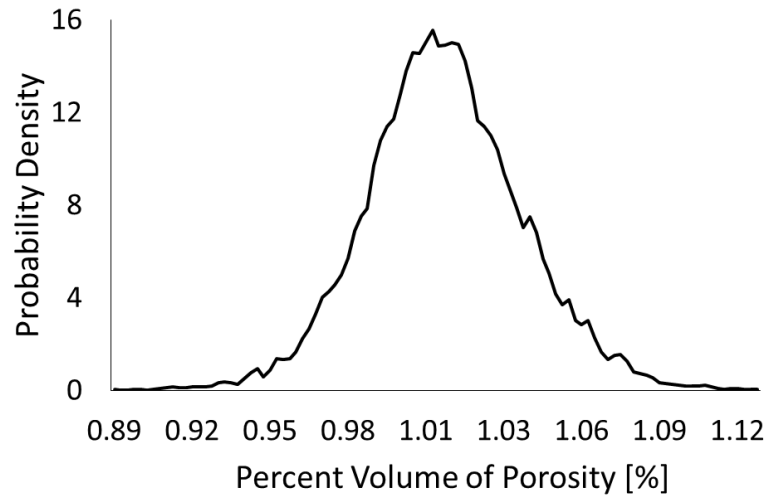
Figure 2.5. Predicted percent volume of porosity PDF with the model uncertainty propagating from uncertain material properties. Despite the 2-5% uncertainty in each thermophysical property, the model predicts a narrow distribution of predicted porosity levels: $1.01\% \pm 0.03\%$.

2.4.2   Fraction Liquid in Multiple Solidification Times

The typical HPDC simulation results for the faction liquid at 12.5s, 15s, 17.5s and 20s are shown in Figure 2.6. In this time sequence, the fraction liquid in casting becomes smaller and the part is fully solid by the 20s ejection time. Based on these results, the position that solidifies last can be determined. The blue packages in images of the casting are the volumes that are not 100% solid at the particular time step. Such volumes are measured and then divided by the total casting volume to yield the percent volume of fraction solid f_s less than 1.
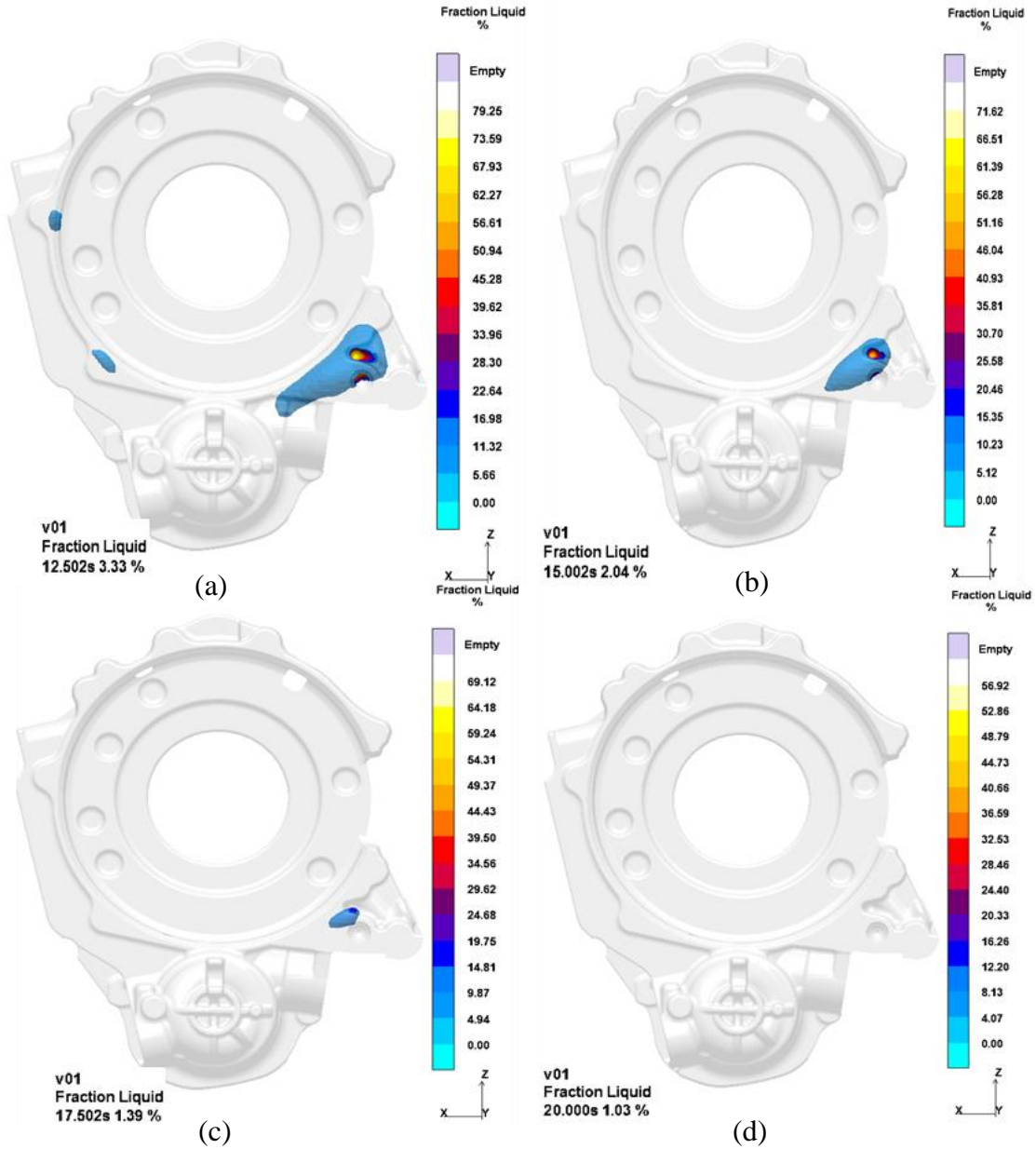
Figure 2.6. Fraction liquid results in (a)12.5s, (b)15s, (c)17.5s, and (d)20s from MAGMASOFT. The blue packages indicate the volume of the fraction solid less than 1.

Figure 2.7 illustrates the sensitivity to the four material properties of predicted percent volume of fraction solid f_s less than 1, which is summarized from the fraction liquid results at each potential solidification time. Although ρ and L_h show the highest

elementary effects, no parameter clearly dominates the sensitivity. Moreover, based on the small magnitude of their elementary effects, the uncertainty in material properties might not significantly affect the fraction liquid result because other deterministic parameters, such as boundary conditions, control the solidification process to a larger extent. With the progression of the solidification process, the elementary effect of k becomes greater than that of C_p. The interaction with other material properties, represented by the error bars in each histogram, describes that the non-linear combined effect from uncertain material properties cannot be neglected.
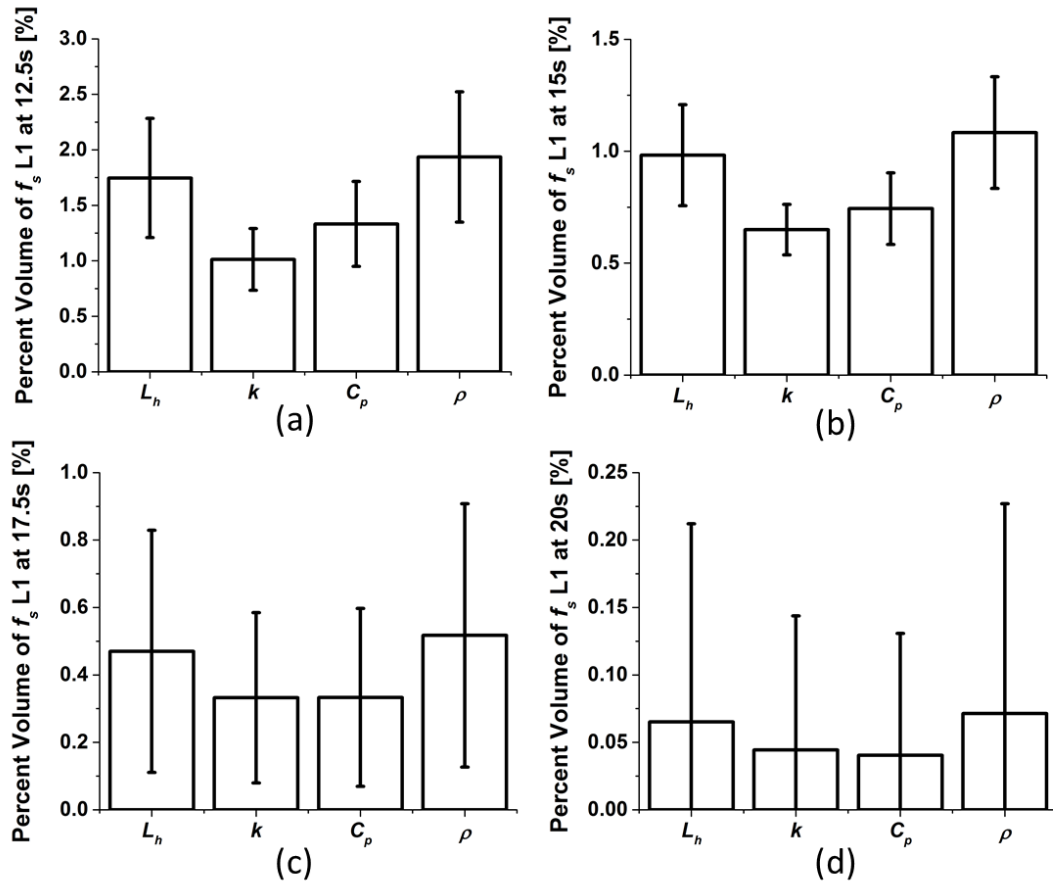
Figure 2.7. Elementary effect of material properties on percent volume of fraction solid (f_s) less than 1 over the uncertain range of material properties at multiple solidification times—(a)12.5s, (b)15s, (c)17.5s and (d)20s. The height of histogram indicates the mean (μ) of elementary effect, and the error bar refers to the magnitude of interaction between material properties.

Figure 2.8 shows the PDFs of predicted percent volume of fraction solid f_s less than 1 collected from the fraction liquid results from MAGMASOFT. All PDFs are calculated from quadratic polynomial surrogate model based on level 2 Smolyak grid sampling algorithm. The HPDC simulation model has a lower limit for the fraction liquid volume result of zero, however the surrogate model that fits to the sampling data by polynomial method has no such restriction. Therefore, the resultant PDFs might have negative value for the non-solid volume for certain sets of input parameters. Such

negative results are manually dismissed in this work and the non-solid volume is assumed

to be zero, which means the casting has become 100% solid. As the solidification process

continues, undoubtedly the non-solid volume in casting becomes smaller and ultimately

disappears. The distribution of PDFs become more concentrated around their means as

the solidification process continues and the model uncertainty is skewed with a long tail

left of the mean value. This long left tail in each PDF originates from the extreme values

of inputs which are represented by the tail in the Gaussian distribution of uncertain

inputs. By integrating the negative PDF in the range of the negative value, the probability

of 100% solid case in certain solidification time is determined. Similarly, the probability

of 99% and 98% solid cases are also obtained by the integration of PDF in particular

percent non-solid volume range. All probability results in multiple solidification times are

shown in Figure 2.9. It refers to the reliability of the casting ejection time in HPDC

process. With uncertainty in the material properties, it is impossible to ensure every

casting product is 100% solid at the 20s ejection time, but the 98% or 99% solid criteria

can be met.
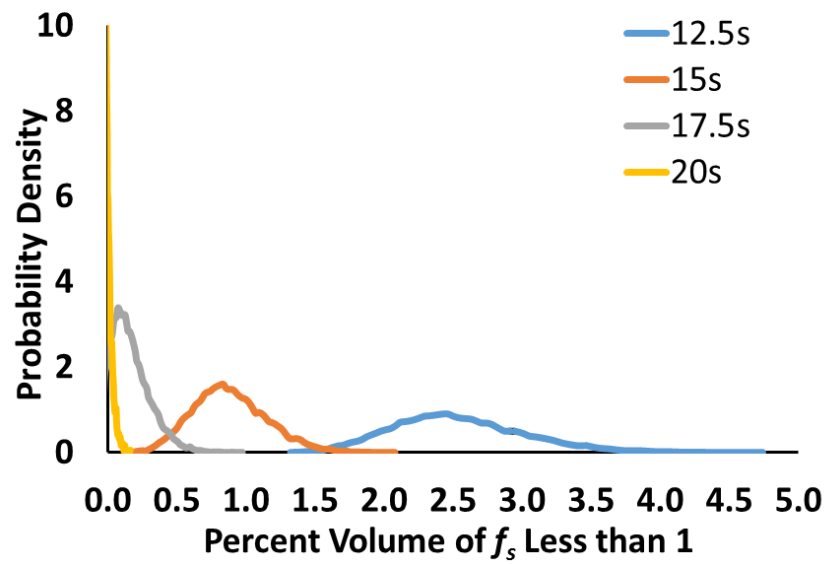
Figure 2.8. PDF of percent volume of fraction solid (f_s) less than 1 at multiple solidification times in the uncertainty quantification on material properties. As solidification process continues, the fraction liquid decreases and the PDF becomes more concentrated. The negative values predicted by surrogate model are manually neglected here, but indicate completely solid parts.
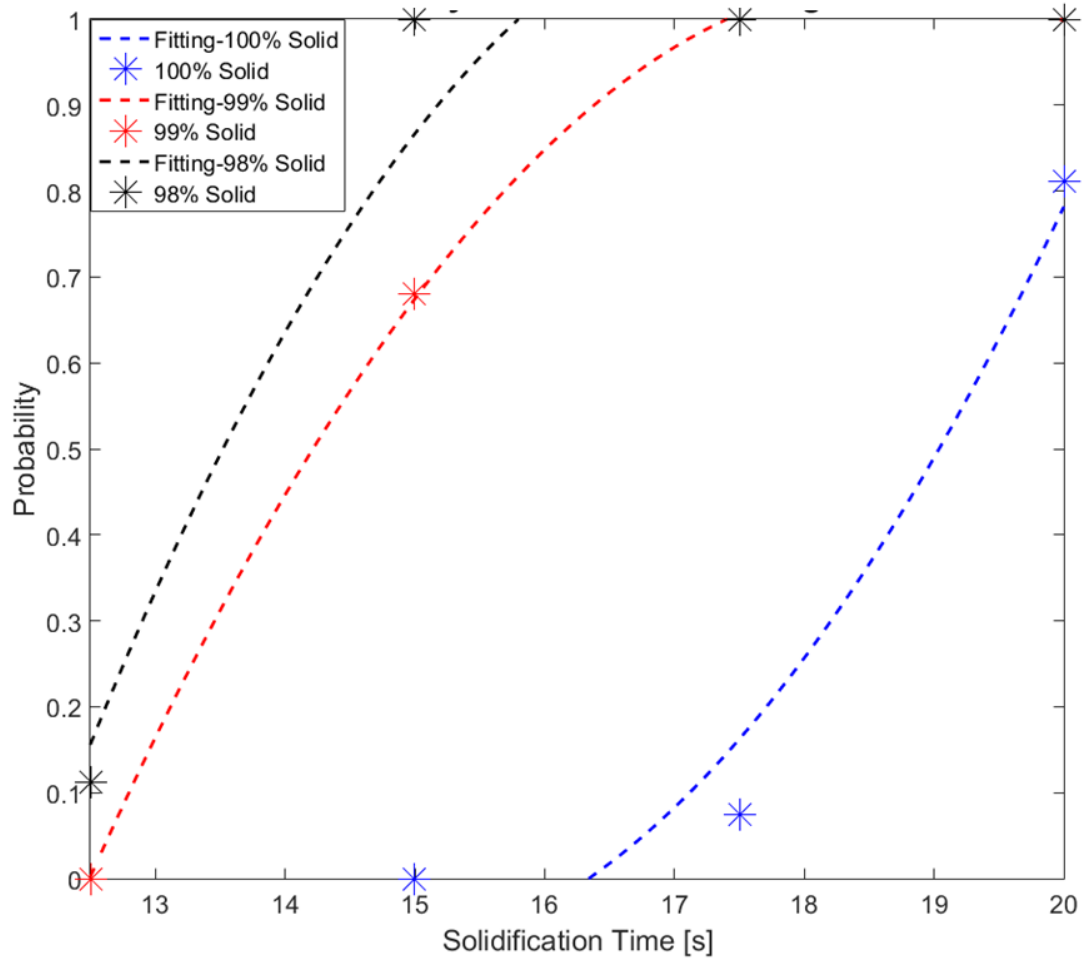
Figure 2.9. Probability of obtaining a solid or mostly solid part at a given solidification time. Blue points indicate the probability of obtaining 100% solid casting at multiple solidification times, red points indicate the 99% solid and black points indicate the 98% solid. Dashed lines with the same colors are to guide the eye. These probability values at different solidification times are obtained by integrating the PDFs with percent volume of f_s less than 1.

CHAPTER 3. UNCERTAINTY QUANTIFICATION ON BOUNDARY CONDITIONS IN HPDC

3.1 Introduction of Experiment

In HPDC industrial process, the solidification model is greatly affected by the boundary conditions. These boundary conditions determine the speed of the solidification process and where the defects, such as porosity, exist. Each boundary conditions in the HPDC models of MAGMASOFT is represented by a Heat Transfer Coefficient (HTC). It can be a constant, which means the cooling condition does not change during the simulation, or be a function of time or temperature, which represents a transient cooling phenomenon.

There are four kinds of boundary condition in HPDC solidification simulations. The first type is the environmental boundary condition, which occurs at the outermost interface between the mold and the surrounding air. The environmental HTC values are at least two magnitudes smaller than any of the other boundary conditions. Therefore, the uncertainty in the environmental boundary condition is neglected in this analysis because it has negligible impact on the simulation results.

The second type is the interface between the cooling channels and the casting dies. The cooling channels in the ejector die, for example, are shown in Figure 3.1 (a). Although these cooling channels do not contact the casting directly, they remove most of the heat released from casting metal out of the dies and might significantly control the

cooling. Thus, the HTC values for the cooling channel should be evaluated as accurately as possible in the simulations.

(a)   (b)
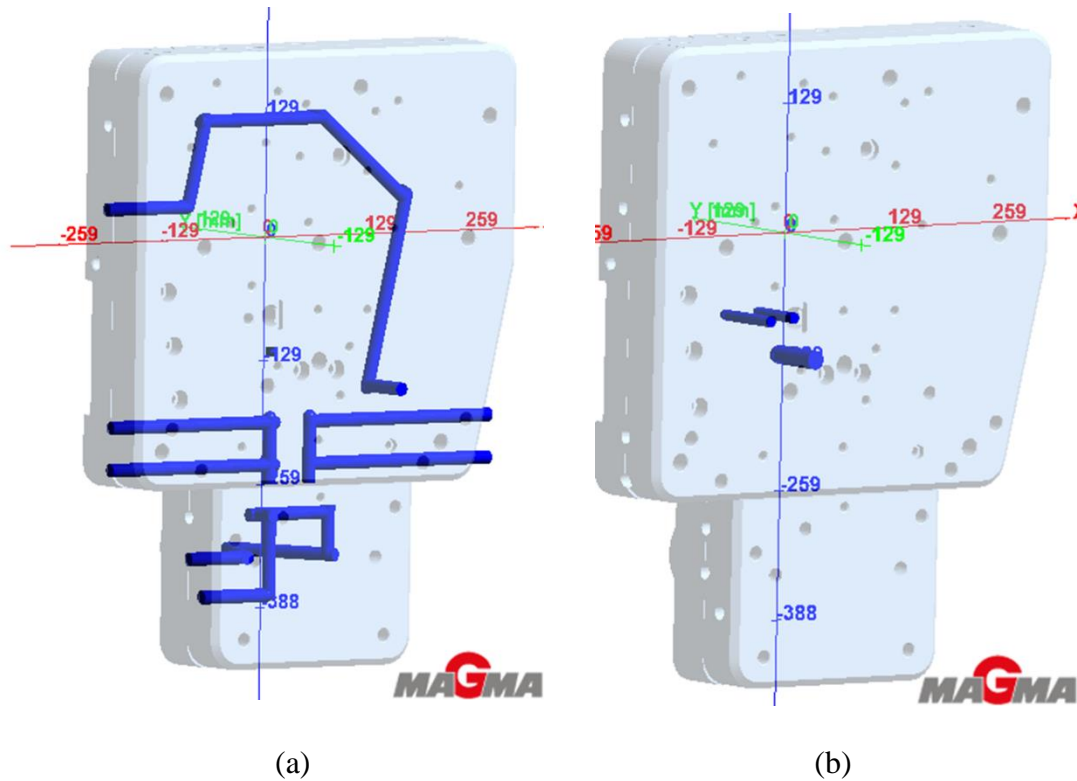
Figure 3.1. (a) Cooling channels in ejector die, (b) Cooling jet units in ejector die.

The third type of boundary condition, occurs at the interface between cooling jet units and the dies. Although very similar to the previous boundary conditions, these cooling jet units are distinguished from the cooling channels by the installation and inner structure. Cooling channels are drilled through from one side to the other so that the coolant can be delivered corresponding to the channel path, while cooling jet units are installed in blind holes which are perpendicular to the side of dies, with a tiny inner tube located in the center of each unit. Essentially, the cooling jets are intended to provide the localized cooling at particular points in the structure. Examples of cooling jet units

installed in ejector die are displayed in Figure 3.1 (b). The tip of cooling jet unit is often arranged as close to the casting cavity as possible so as to accelerate the heat removal rate for local casting position. The coolant is injected into the cooling jet unit through the tiny inner tube, back from the tip of cooling jet unit and out of the unit in the annular section. A detailed cross-section of this cooling jet unit structure is displayed in Figure 3.2, in which d is the diameter of inner tube, D is the diameter of cooling jet unit and S is the length of tip. Due to its structure characteristics, the cooling jet unit is divided into three different zones, each of which has an individual HTC value because of the different local heat transfer mechanism. Zone 1 is tip area where the coolant is just out of the nozzle and has not returned back to the annular area. Zone 2 and 3 are the annular areas but process different HTC values as the flow progresses down the channel.

The fourth kind of boundary condition is the air gap interface between the metal and die, which is the most difficult parameter to determine. The air gap evolves over time as the metal shrinks during the liquid-solid phase change process. The density of liquid phase of metal is smaller than that of solid phase. Thus, during solidification, the density change leads to shrinkage pores inside the casting, as well as contraction from the die surface that leads to the final formation of air gap between the casting and the dies. Since the solidification process of HPDC is fast and this boundary condition is directly exerted at the surface of the casting, the HTC of metal-die gap is expected to play a significant role in the HPDC simulation results.
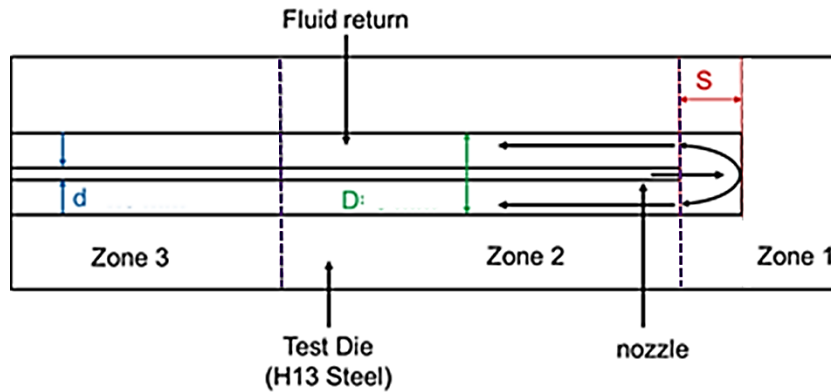
Figure 3.2. Schematic of cooling jet unit installed in the test die. A small inner tube inside the cooling jet unit is a guide tube that leads the coolant to flow into the unit. *Zone 1* indicates the tip area from which the coolant is out of the nozzle. *Zone 2* and *3* are the annular areas in which the coolant flow back.

The uncertainty quantification of this experiment focus on the last three kinds of boundary conditions, which represent the effect of the cooling channels, cooling jet units and metal-die air gap on the HPDC process. The material properties in this experiment are the mean values applied in the uncertainty quantification of material properties without considering their uncertainties. Except the variation of boundary conditions discussed here, other parameters in MAGMASOFT remain unchanged.

3.2   Inputs of Interest

For the three kinds of boundary conditions, four types of HTC values or curves with their aleatory uncertainties are considered as inputs of interest for uncertainty quantification of boundary conditions of HPDC. As described in more detail below, three of these come from the heat transfer correlations summarized from experimental data and the final one is calculated by numerical methods from related temperature measurements in literature.

3.2.1 HTC of Cooling Channel

The first input is the HTC value representing the impact of the cooling channels. Since

the coolant, which is water in practice, inside these tempering channels is driven by a

pump with external high pressure, its velocity is so large that turbulent flow determines

the characteristic of boundary condition of cooling channels. Due to the large ratio of

length to diameter of channel, the hydrodynamic entrance region is small enough to be

neglected and the turbulent flow is considered as fully developed through the whole

channels. Thus, for fully developed turbulent flow in a horizontal smooth circular tube,

the local Nusselt number Nu_D may be obtained from the Dittus-Boelter correlation for

cooling (as the wall temperature around cooling channel is higher than coolant

temperature) [7, 35]:

$$Nu_D = 0.023Re_D^{0.8}Pr^{0.3}, \tag{3}$$

where Re_D is the Reynolds number based on the diameter D and Pr is the Prandtl number.

Although the complex cooling channel arrangement leads to both upward and downward

turbulent flow, the Dittus-Boelter correlation is still applicable but fits with at best 20%

uncertainty against experimental data [36]. The water circulated inside the cooling

channel is about 25 ℃, thus its Prandtl number is about 5.83. Given the diameter of

channel tube and water flow parameter, the HTC of cooling channel boundary condition

is calculated by Equation (3) to be as 8000 $W/_{m^2K}$. Assuming there is no other

uncertainty for the variables in Dittus-Boelter correlation equation except the correlation

fitting uncertainty, the total uncertainty of the calculated HTC of the cooling channel

boundary condition is 20%.

3.2.2   HTCs of Cooling Jet Unit

The second and third inputs of interest are the HTC values representing the

cooling effect of cooling jet unit zone 1 and 2 respectively. As displayed in Figure3.2,

Zone 1 is the tip area close to the casting cavity. Zone 2 and 3 are annular areas that lead

the cooling water out of the jet unit. Although the local HTC values of zone 2 and 3 are

different, the location of zone 3 is sufficiently far away from the casting cavity that it is

expected to have a small impact on the HPDC solidification process of casting in

comparison with zones 1 and 2. Therefore, only the HTCs for zones 1 and 2 of cooling jet

units, shown in Figure 3.3, are considered to have uncertainty in the simulation and the

HTC boundary condition values are set as inputs of interest that might determine the

HPDC simulation results.

In order to obtain the HTC values, a two-dimensional control volume method was

applied to experimental data in the calculations of heat flux q'' and the average HTC

value $\bar{h}$[37, 38]. As illustrated in Figure 3.4, at least five thermocouples are needed to

obtain the HTC from transient temperature data. Then, the heat flux as and the average

HTC value of each zone are calculated by

$$q'' = \frac{1}{A_x}\left[k\left(\frac{A_x\Delta T_2}{\Delta x} + \frac{A_y\Delta T_3}{\Delta y} + \frac{A_y\Delta T_4}{\Delta y}\right) + \rho C_p \Delta V \frac{\Delta T_t}{\Delta t}\right] \qquad (4)$$

where the ΔT_n is evaluated as $T_1 - T_n$ and ΔT_t is the difference of temperature at point

one between the current and previous time step. Thus, from Newton's Law of Cooling:

$$\bar{h} = \frac{q''}{T_{water}-T_1}, \qquad (5)$$

where T_{water} is the temperature of cooling water in the jet unit.
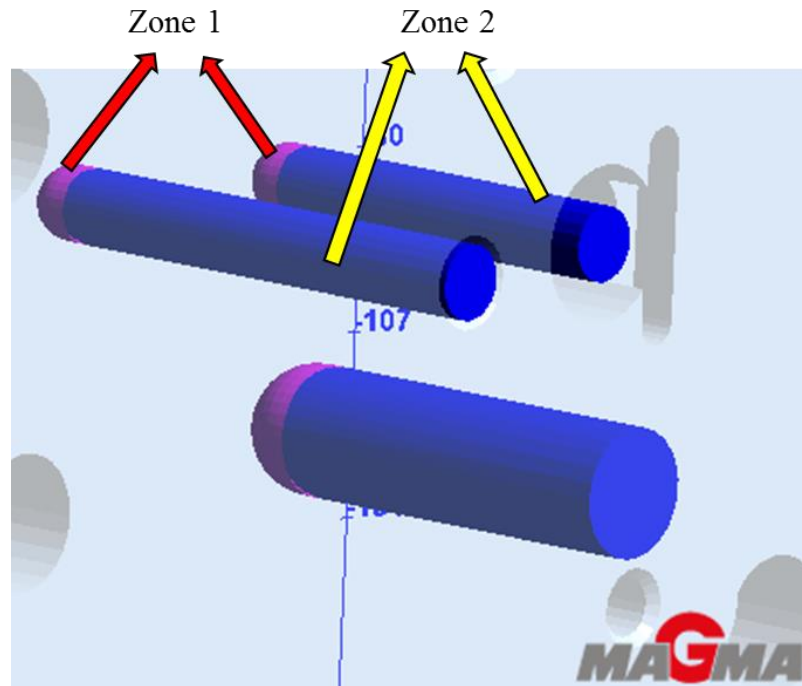
Figure 3.3. Schematic of cooling jet unit Zone 1 & 2 in MAGMASOFT. The purple tip denotes the area of appropriate HTC of Zone 1, while the blue tube surface denotes the area of appropriate HTC of Zone 2.
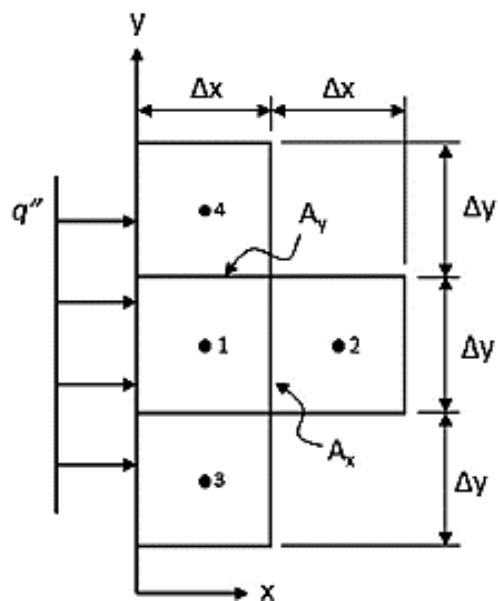
Figure 3.4. Schematic of the 2-D Control Volume Method from Plotkowski *et al* [38].

In order to correlate the average HTC values for zones 1 and 2 into an equation of the form: $\overline{Nu_x} = f(Re_x, Pr)$ or $\overline{Nu_D} = f(Re_D, Pr)$, series of experiments performing heat transfer measurements under controlled laboratory conditions were conducted by Poole and Krane. The coolant water was at 20°C, with a known Pr value. Considering that the geometry of cooling jet unit might impact the average HTC value, the ratio of the length of tip to the diameter of nozzle, S/d, were varied, in addition to varying the Re_x. The positions of thermocouples in the zone 1 and 2 were arranged as shown in Figure 3.5. Results of experiments are shown in Figure 3.6 and 3.7 and correspond to the correlations for zone 1 and zone 2, respectively.
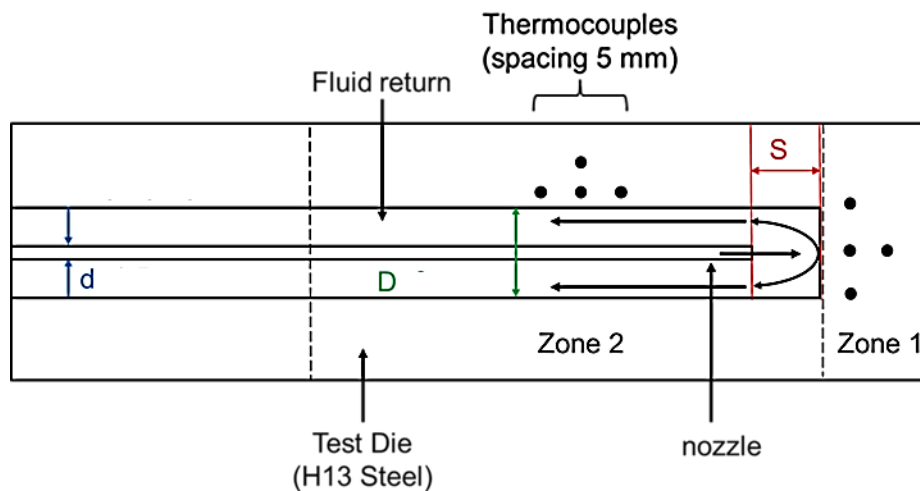
Figure 3.5. Schematic of thermocouples in correlation experiment done by Poole and Krane. Two groups of five thermocouples are arranged around the tip and annular areas, respectively. The HTC values of Zone 1 and 2 are calculated based on the temperature data of these thermocouples.
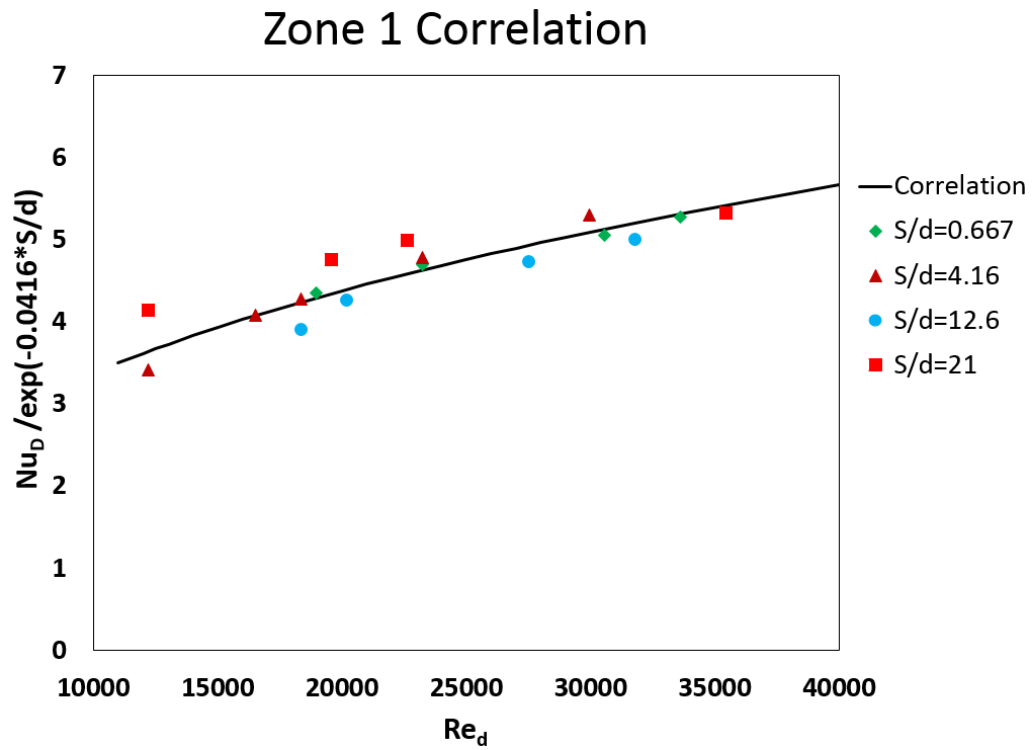
Figure 3.6. Heat transfer coefficient correlation for Zone 1. Symbols with different shapes and colors denote different geometries of the cooling jet unit. The correlation as a function of Re_d is displayed in a solid line with the RMSE $\pm$ 0.245.
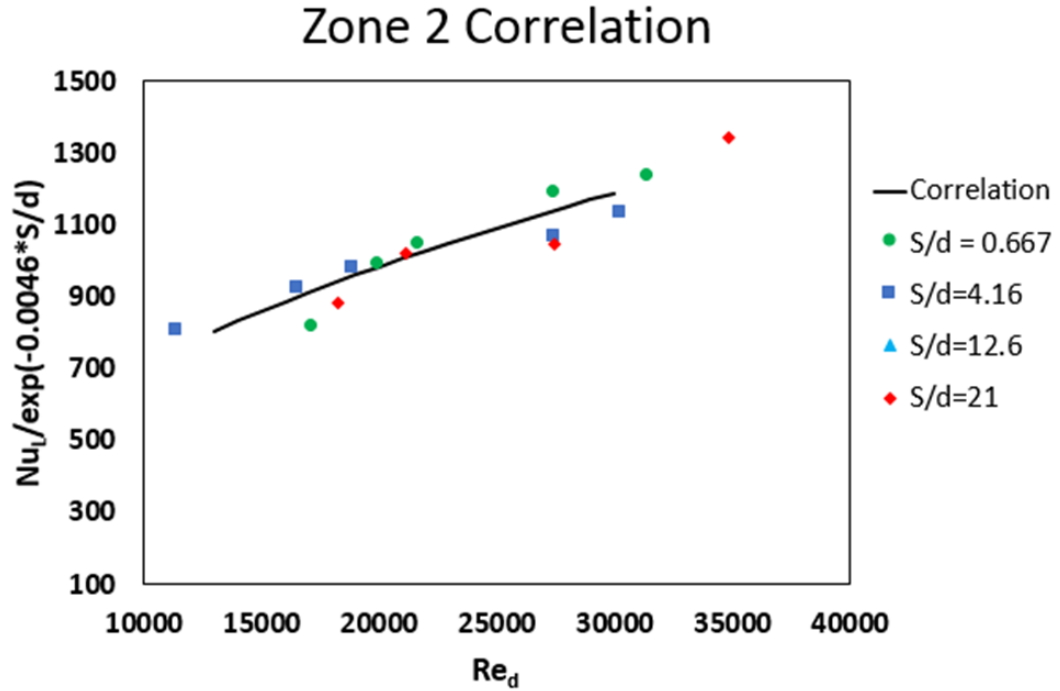
Zone 2 Correlation

Figure 3.7. Heat transfer coefficient correlation for Zone 2. Symbols with different shapes and colors denote different geometries of the cooling jet unit. The correlation as a function of Re_d is displayed in a solid line with the RMSE $\pm$ 53.32.

Based on these results, the cooling jet unit geometry indicator, S/d, has negligible influence on the correlation for the heat transfer performance in both zones 1 and 2. Therefore, the effect of geometry on the correlation is neglected and the correlation is considered to be simply determined by the Re value. All the experimental results accumulated in zone 1 are fitted by the following correlation:

$$\frac{Nu_D}{e^{\left(-0.0416*\frac{S}{d}\right)}} = f(Re_d). \tag{6}$$

Similarly, the results collected in zone 2 are fitted by following correlation:

$$\frac{Nu_L}{e^{\left(-0.0046*\frac{S}{d}\right)}} = f(Re_d). \tag{7}$$

The HTC values calculated from both correlations are significantly different. Given the S/d ratio of industrial cooling jet units in HPDC process and the Re number calculated based on the coolant velocity inside, the calculated HTC value in zone 1 is 235 W/m^{2}K, significantly smaller than the 3510 W/m^{2}K predicted in zone 2. However, considering zone 1 is the area around the tip of the cooling unit very close to the casting, it might still have an important impact on the HPDC simulation results. The area of zone 2, which is a little further away from the casting cavity, might also play a significant role in HPDC casting because of the larger HTC quantity. The uncertainty of each correlations is the Root Mean Square Deviation (RMSD) calculated simultaneously in data fitting process. The RMSD of the correlation in zone 1 corresponds to 14 W/m^{2}K while that in Zone 2 is 214 W/m^{2}K. They are considered as the aleatoric uncertainties in the following uncertainty quantification investigation.

3.2.3 HTC Curve of Metal-die Interfacial Air Gap

The fourth and final input of interest is the interfacial heat transfer coefficient (IHTC) representing the effect of the air gap between the casting and the die. This IHTC curve, as a function of time, is believed to be one of the most essential boundary conditions in HPDC process since it directly controls the solidification process. In order to obtain accurate boundary conditions between the casting and mold, inverse methods are widely applied in the calculation of IHTC curve [39, 40, 41]. Given the measured temperature history inside a heat-conducting solid, the surface temperature of mold $T_{mold\ surface}$ and heat flux density q'' can be calculated by a numerical process. Then, the

IHTC is obtained by the Newton Cooling law if the casting temperature $T_{casting\ surface}$ is known as:

$$h = \frac{q''}{T_{casting\ surface} - T_{mold\ surface}}. \tag{8}$$

The inverse method has been successfully applied in the IHTC curve calculation in sand casting [42] and squeeze casting [43]. Both of these works have a thermocouple installed inside the casting cavity for the measurement of temperature of the casting surface. However, for the HPDC process, it is not possible to install a thermocouple inside the casting cavity because the guide hole to the cavity for the thermocouple will ruin the die and finally lead to the liquid metal leakage in the HPDC process. Instead of the direct measurement of casting surface temperature, a simplified 1-D energy balance Equation (9) with phase change is assumed in the casting domain:

$$\rho c_p \frac{\partial T}{\partial t} - \frac{\partial}{\partial x}\left(k \frac{\partial T}{\partial x}\right) = \rho L_f \frac{\partial f_s}{\partial T}, \tag{9}$$

where f_s is the fraction solid of the casting and the term $\partial f_s / \partial T$ is determined by solidification curve calculated based on thermodynamic principles. If the shape of casting is symmetric, adiabatic boundary conditions can be applied in the center line of casting. The boundary condition in casting surface is the heat flux density q'' calculated by inverse method. With both boundary conditions, the 1-D transient temperature distribution of casting, including the temperature data in the surface, can be predicted. Therefore, the HTC curve as a function of time can be derived by Equation (8). The scheme of the whole numerical model is shown in Figure 3.8. The thermocouple positions of Tc1, Tc2 and Tc3 are arranged for the temperature measurement.
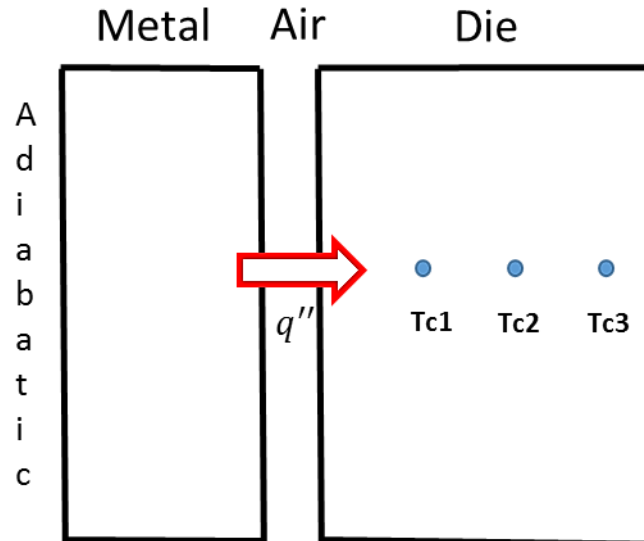
Figure 3.8. Schematic of 1-D Inverse Method. Tc1,2 and 3 are the thermocouple positions with the same distance from each other. The temperature data from Tc3 is used as the boundary condition for the calculation of the heat flux q'' and temperature at die surface. With the calculated q'' and an assumed adiabatic boundary condition at the center of casting metal, the temperature at the metal surface is calculated and the IHTC value at particular time can also be obtained by Newton Cooling law.

In past work, the IHTC curve in HPDC process was successfully obtained by the numerical calculation of inverse method in the die domain and 1-D energy balance model with phase change in the casting domain [44, 45, 46]. The numerical result shows that the IHTC increases very quickly during the liquid metal filling process until it reaches the peak, and then it drops smoothly to a lower level. After this level is reached, the value of IHTC keeps roughly constant in the following solidification process. Thus, the response of the IHTC value from filling to solidification process corresponds to three steps: (1) *the plunge filling step,* in which the liquid metal has just been injected by the external high pressure and contacts the die surface tightly. Good contact between the liquid metal and die leads to the abrupt increase of IHTC value in a short time. (2) *The beginning of*

solidification at the surface of casting. The phase change from liquid to solid leads to shrinkage of the casting and finally results in the formation of an air gap. The air gap dominates the thermal resistance between the casting and the die. Thus, during the formation of air gap, the IHTC value decreases smoothly since the casting is losing the contact with die because of shrinkage. (3) *The time after the formation of the air gap*. In this step, the phase transformation at the surface of the casting has finished but the solidification in the inner part is not yet complete. In this phase, the solidification process continues with the air gap remaining fairly constant. Therefore, the IHTC value maintains roughly the same value.

Many parameters in HPDC process influence the result of the IHTC curve. First, different types of casting material lead to a great variation of IHTC curves [44], since the density difference between liquid phase and solid phase are not the same and leads to the variations in the air gap formation. Second, the thickness of casting affects the shape of IHTC curve since it greatly changes the flow profile during the filling process [45]. Third, filling velocity, determined by plunge shot speed, has a great impact on the peak IHTC value. Further, the initial die surface temperature also has an effect on the peak IHTC value. Even for a casting sharing the same thickness everywhere, the filling sequence, beginning in gate, and ending in overflow position, also affects the shape and peak value of IHTC curve [46]. After the comparison of the effect of all parameters on IHTC curve, the impact of the type of casting material is most significant because both shape and peak value of IHTC are greatly affected by the variation of the air gap formation determined by density change. Thus, in order to have an IHTC curve as

accurate as possible for A380 HPDC simulation, such curves should be obtained from the real experiments with A380 HPDC.

A new non-intrusive measurement method using an infrared probe was recently applied to obtain the IHTC curve of A380 HPDC process [47, 48]. The uncertainty of the IHTC curve is found to be a maximum of 30%, coming from a combination of experimental uncertainties. Figure 3.9 (reproduced from [48]), displays the IHTC curve as a function of time in black line with 30% uncertainty as two dash lines. The peak of the IHTC is 90,000 W/m^2K(see the a purple dashed dot line in Fig. 3.9) and this peak indicates the separation of the filling process and solidification process. The IHTC value characterizing a stable air gap between the casting and the die is 5000 W/m^2K, which begins from 1s to the end of the solidification time. This IHTC curve is applied as the metal-die boundary condition in this uncertainty quantification.
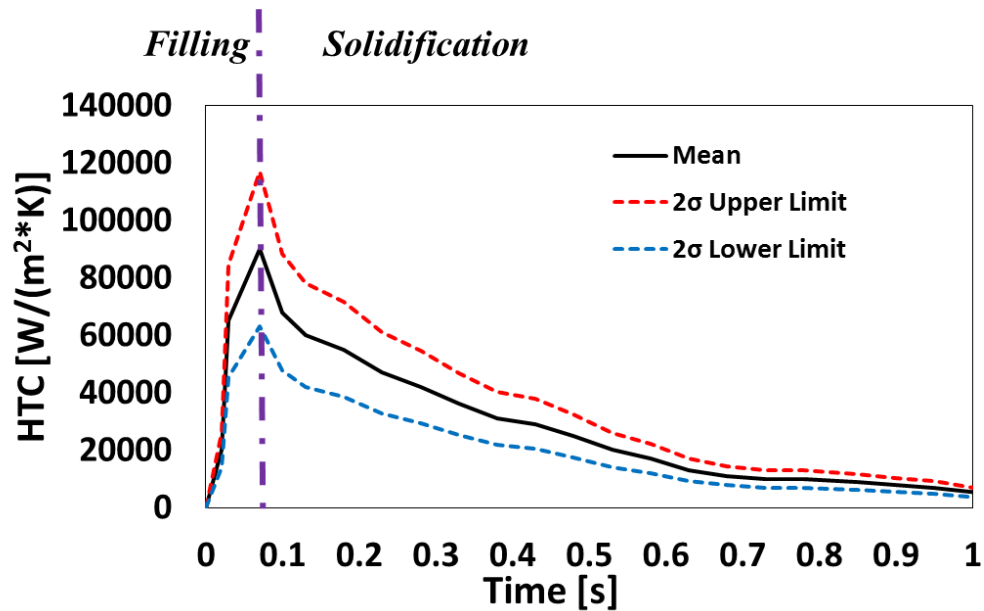
Figure 3.9. Metal-die interfacial HTC as a function of time. The black line is experimentally-derived HTC curve (mean) from Dargusch *et al* [47]. The two dash lines are 30% (2σ) away from the black curve, representing a Gaussian distribution of uncertainty. The purple dash dot line indicates the separation of the filling process and solidification process.

3.3   Process of Uncertainty Quantification

Four boundary condition values—HTC value of cooling channel, HTC value of zone 1 and 2 of cooling jet unit, and IHTC curve of air gap—with their uncertainties are considered as the inputs of interest in this uncertainty quantification investigation. These four inputs are submitted to the PUQ framework to obtain the required sampling cases for the generation of the surrogate model, and output PDFs. Since the boundary condition between the casting and the die is a function of time, it is first normalized to one unit so that it can be submitted to PUQ framework as a single value. The uncertainties of four boundary conditions are all considered to be represented by Gaussian distribution since they come from the experimental error with confidence in precision. Therefore, the deviation (σ) of Gaussian distribution submitted to the PUQ framework should be half of

the uncertainty value of boundary conditions respectively so that 2σ represents 95%

confidence in the experimental precision. In this uncertainty quantification investigation,

only aleatoric uncertainty from the experimental measurement is considered, and the

epistemic uncertainty from experimental methodology is dismissed. All of the boundary

conditions with their uncertainties as input of interest are summarized in Table 3.1

Considering the potential interaction of these four boundary conditions in HPDC process

simulation in MAGMASOFT, a level 2 Smolyak algorithm is applied in the sampling

process. Total 41 sampling cases are generated, each of which has its own input

parameters as MAGMASOFT simulation setting. After simulating these 41 cases, the

results of the outputs of interest are accumulated and submitted to be PUQ framework

again to obtain the surrogate model and output PDFs.

Table 3.1 Inputs of Interest for Uncertainty Quantification on Boundary Conditions.

Boundary Condition		Mean Value or Normalized Mean(μ)	2σ
Cooling Jet Unit	Zone 1	235	28
	Zone 2	3510	428
HTC of Cooling Channel		8000	1595
IHTC Curve of Metal-die Air Gap		1	0.3μ

3.4   Outputs of Interest

In this uncertainty quantification of boundary conditions, the percent volume of

porosity and the fraction liquid at multiple solidification times are considered as the

outputs of interest, as previously described in Chapter 2. A comparison of the results

between the two uncertainty quantification investigations is discussed in the following results and analysis section.

3.5 Results and Analysis

3.5.1 Porosity

The typical HPDC simulation porosity result from MAGMASOFT is shown in Figure 3.10. The blue packages in the figure are the potential volumes in which the shrinkage pores might form. Note that the simulations in this chapter are based on the experimentally-derived HTCs, which in chapter 2, the HTCs are default MAGMASOFT settings. Comparing the shrinkage packages in Figure 3.10 with the ones in Figure 2.3, the positions are qualitatively similar, but the sizes are slightly different.
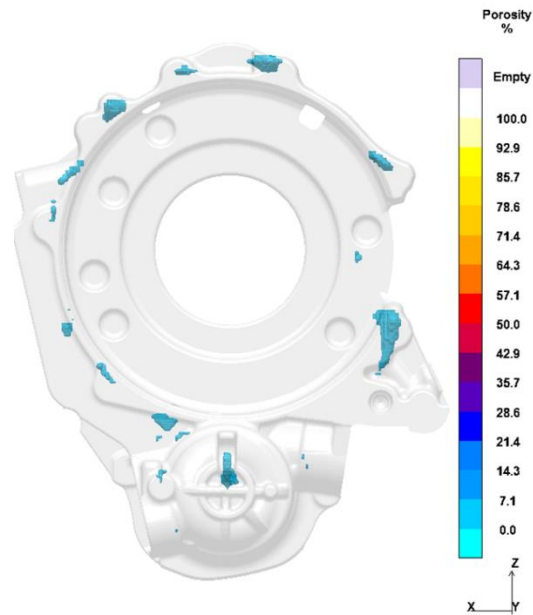
Figure 3.10. Porosity result from MAGMASOFT with experimentally-derived boundary conditions. The blue packages indicate the possible volumes in which the shrinkage pores form.

Figure 3.11 gives the sensitivity of the predicted porosity to the uncertain HTC values for boundary conditions. CJUZ1 and CJUZ2 are the short name of cooling jet unit zone 1 and 2 HTCs, respectively, CCHTC represents the cooling channel HTC, and IHTC indicates the interfacial HTC curve of the air gap between metal and die. From the sensitivity analysis of these four uncertain boundary conditions, the elementary effect of IHTC on the porosity result overwhelms the ones of other three. Compared with 0.81% elementary effect of IHTC on the porosity volume, the effects of other boundary conditions are negligible. In comparison to the elementary effect of uncertain material properties (see in Figure 2.4), the elementary effect of the IHTC is larger than the uncertainty to any of the material properties. The long error bar in the IHTC histogram represents the great non-linearity in the response from the interaction with other boundary conditions.

The resultant PDF calculated from level 2 quadratic polynomial surrogate model for predicted porosity volume is shown in Figure 3.12. The RMSE of surrogate model is 3.92%, which mean the surrogate model is accurate enough to replace the original computationally expensive MAGMASOFT model for calculation of the PDF generation. The PDF describing the model uncertainty is skewed (with a tail towards larger volumes) with a mean (μ) of 1.30% and a deviation (σ) of 0.11%, which constitutes an uncertainty ($^{2\sigma}/_{\mu}$) of 16.9% for predicted porosity. This 16.9% uncertainty in porosity due to uncertain boundary conditions is nearly three times larger than the 5.9% uncertainty propagating from uncertain material properties. That means the uncertain boundary conditions have greater impact on the predicted porosity result. Since the solidification rate during casting is greatly influenced by the HTCs, it is not surprising

that the formation of shrinkage pores during the solidification process is strongly affected

by the boundary conditions. From the sensitivity analysis of all four boundary conditions,

the IHTC has the greatest elementary effect on the predicted porosity result. Thus, the

majority of the uncertainty in the resultant PDF actually propagates from the uncertainty

of IHTC. In order to effectively improve the precision of the predicted porosity result,

improving the accuracy of the IHTC curve should be the first priority.
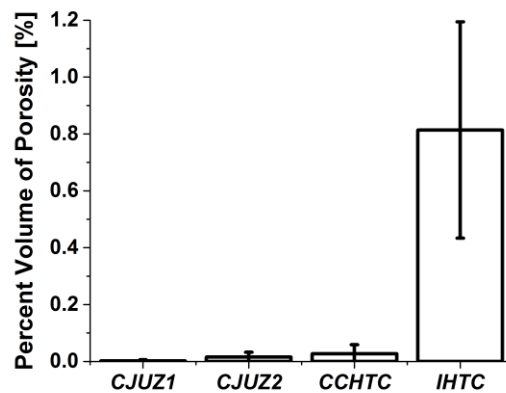
Figure 3.11. Elementary effect of boundary conditions on the percent volume of porosity result. The height of the histograms of *CJUZ1* (the HTC for the cooling jet unit in zone 1)*, CJUZ2* (the HTC for the cooling jet unit in zone 2)*, CCHTC* (the HTC for the cooling channels) and *IHTC* (the interfacial HTC for the die-part interface) represent the mean (μ) of elementary effect over the uncertainty range of the HTCs. The error bars for each histogram indicates magnitude of the interaction on the porosity result between boundary conditions.
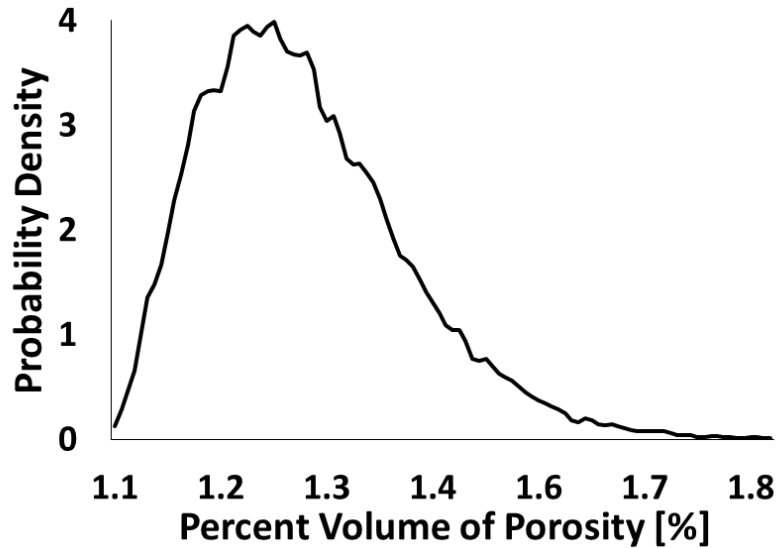
Figure 3.12. Predicted percent volume of porosity PDF with the model uncertainty propagating from uncertain boundary conditions. With appropriate uncertainty in each boundary condition, the model predicts a distribution of predicted porosity levels: $1.3\% \pm 0.11\%$.

3.5.2 Fraction Liquid in Multiple Solidification Times

Typical HPDC simulation results for fraction liquid at 12.5s, 15s, 17.5s and 20s are shown in Figure 3.13. In the time sequence, the fraction liquid in casting becomes smaller as the solidification occurs. Since four boundary conditions have been changed in this uncertainty quantification investigation, in Figure 3.13, the positions and sizes of the blue packages representing the volumes that have not become 100% solid, are different from the ones from the material properties uncertainty quantification previously shown in Figure 2.6. That highlights that the fraction liquid result is directly affected by the boundary conditions because they control the solidification rate of the casting to a large extent. The volumes of blue packages in fraction liquid result are calculated for every sampling simulation cases for the following uncertainty quantification analysis.
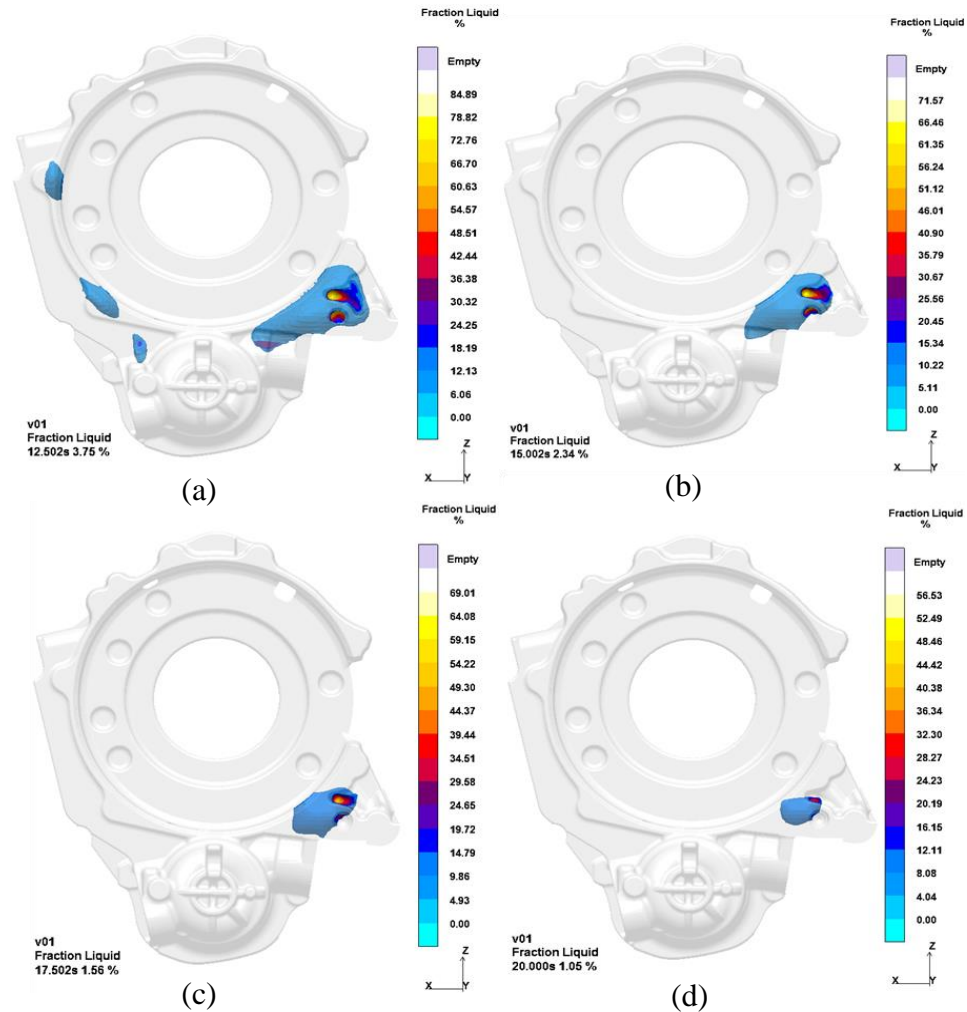
Figure 3.13. Typical Fraction liquid results with experimentally-derived boundary conditions at four times during the solidification process (a)12.5s, (b)15s, (c)17.5s and (d)20s. The blue packages indicate the volume of the fraction solid less than 1.

Figure 3.14 shows the sensitivity of predicted percent non-solid volume, summarized from fraction liquid results at multiple solidification times, for four boundary conditions. The mean (μ) of element effect of IHTC of the fraction liquid results at different solidification times also greatly overwhelms any one of the other three which are so insignificant that can be considered as negligible. This sensitivity result is

reasonable because the IHTC, representing the boundary conditions between the casting and die, directly determines the heat removal rate from the casting, while the other HTCs, representing the boundary conditions of the interface between cooling line and dies, don't have sufficient time for interaction with the casting and they do not control the heat removal rate from the casting directly. Moreover, the elementary effect of boundary conditions on the fraction liquid result are also determined by the efficient working areas.

The IHTC boundary condition impacts the whole casting surface, corresponding to a large area, while the others only impact the area near the cooling lines with small surface areas. Therefore, it is not difficult to conclude that the interfacial boundary condition of air gap between metal and die almost completely controls the predicted fraction liquid. However, the long error bar in the histogram of IHTC indicates that the interaction with other boundary conditions is strong.
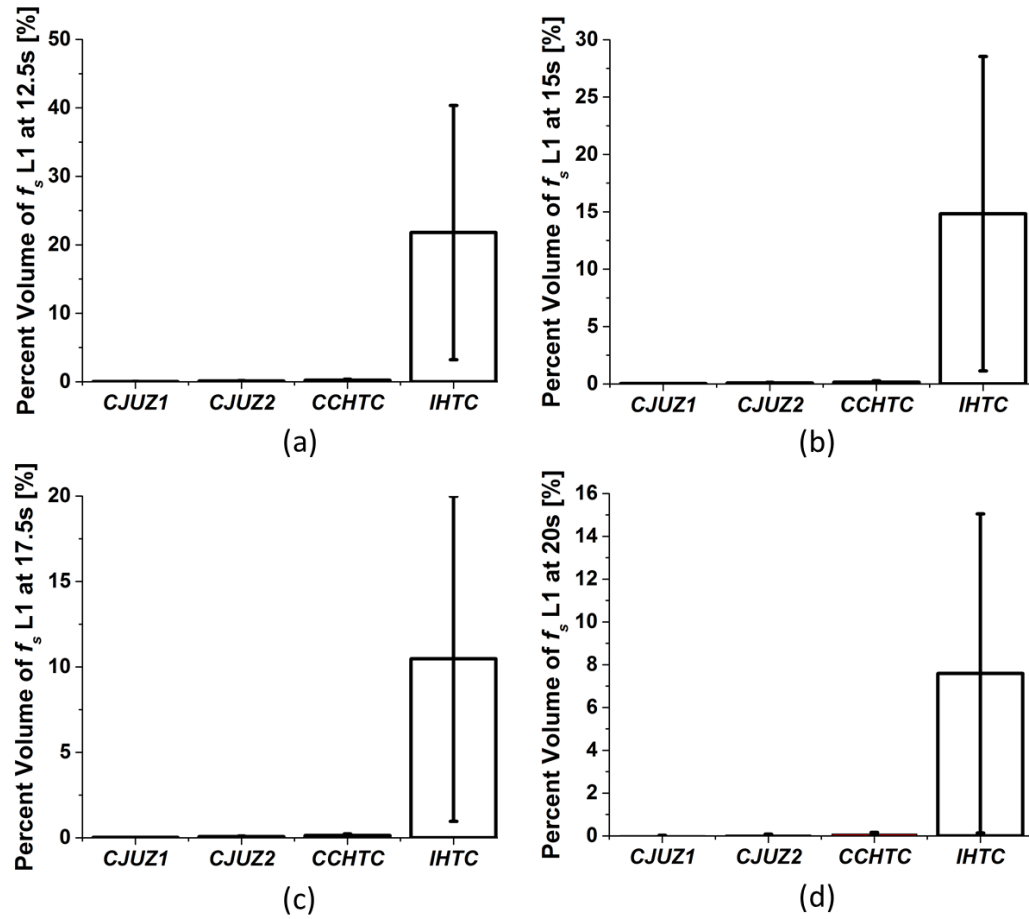
Figure 3.14. Elementary effect of boundary conditions on percent volume of fraction solid (f_s) less than 1 over the uncertain range of boundary conditions at multiple solidification times—(a)12.5s, (b)15s, (c)17.5s and (d)20s. The height of histogram indicates the mean (μ) of elementary effect, and the error bar refers to the magnitude of interaction between boundary conditions.

From the previous sensitivity analysis, IHTC has an overwhelming elementary effect on the fraction liquid results. Thus, the surrogate model can be simplified as a function of normalized IHTC factor while neglecting other three parameters of boundary conditions. As an example, a surrogate model for percent non-solid volume at 20s generated from fraction liquid results is shown in Figure 3.15. The negative results predicted by surrogate model are manually dismissed. The result of this surrogate model clearly demonstrate the significance of the uncertain IHTC curve on the percent volume of fraction solid (f_s) less than 1 at the 20s solidification time. With low IHTC, the model predicts a maximum 7.4% fraction liquid uncertainty at the 20s casting ejection time, while at higher IHTC values, the system has completely solidified highlighting the strong influence of uncertain IHTC boundary condition on the fraction liquid.
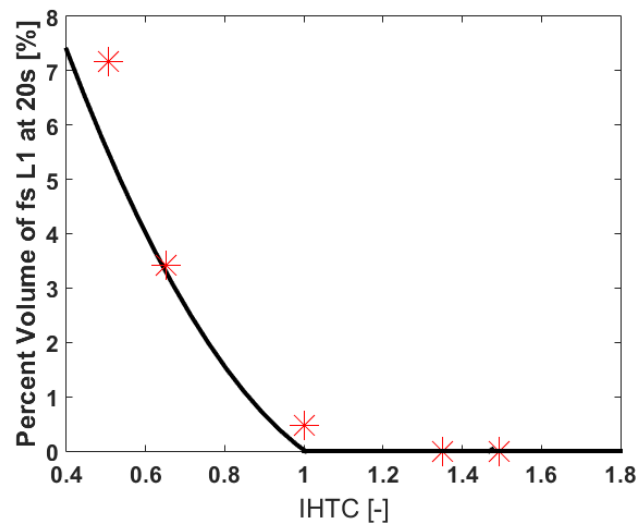
Figure 3.15. Surrogate model as a function of the IHTC factor. Red symbols are the results of sampled cases and the black line is the fitting surrogate model.

Figure 3.16 shows the PDFs for the predicted percent non-solid volume

calculated from the surrogate models of fraction liquid at different times respectively. All

PDFs are calculated from quadratic polynomial surrogates respectively based on level 2

Smolyak grid sampling algorithm. The maximum RMSE among these surrogates is

13.8%. Since the HPDC simulation model has a lower limit in fraction liquid result of

zero and the surrogate model generated by polynomial method has no such restriction, the

resultant PDF might have negative value for the non-solid volume in fraction liquid result

for certain sets of input parameters. Such negative results are manually dismissed in

Figure 3.16 and assumed to be zero for the non-solid volume, which means the casting

has totally finished the liquid-to-solid phase transformation. By integrating the PDF in

the in the range of negative value of percent non-solid volume, the probability that the

casting is 100% solid at multiple solidification times is determined. Similarly, the

probability of 99% and 98% solid case is also obtained by the integration of PDF in the

corresponding range. These three probability results for multiple solidification times are

shown in Figure 3.17 as a reference for the reliability of the ejection time. Note that with

the uncertain boundary conditions, it is impossible to ensure every casting product

reaches 100% solid at the current 20s casting ejection time. Different from the Figure 2.9,

it is also impossible to ensure full confidence in obtaining 99% and 98% solid at the

current ejection time setting. That means the uncertainty in boundary conditions brings

more delay on the casting solidification process.
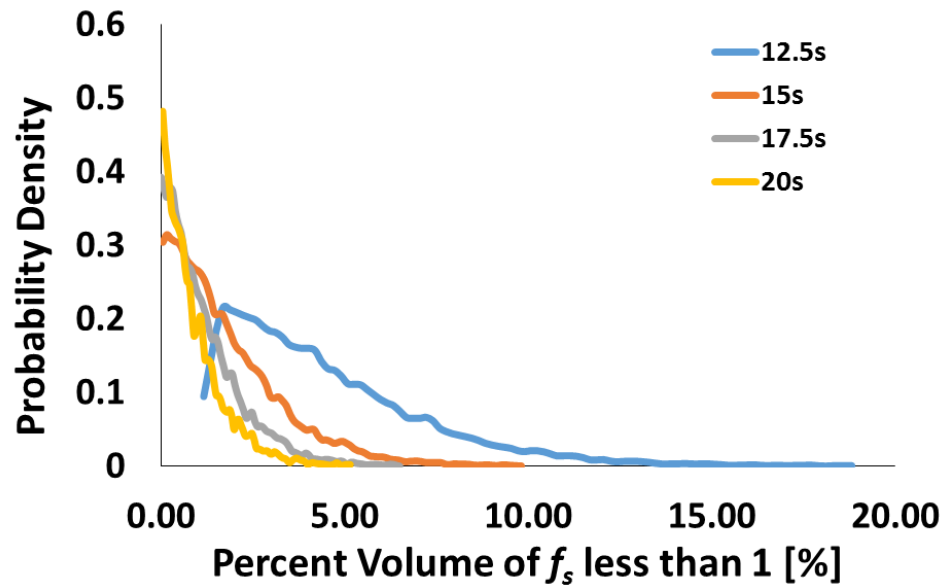
Figure 3.16. PDF of percent volume of fraction solid (f_s) less than 1 at multiple solidification times in uncertainty quantification investigation of boundary conditions. As solidification process continues, the fraction liquid decreases. The negative values predicted by surrogate model are manually neglected.
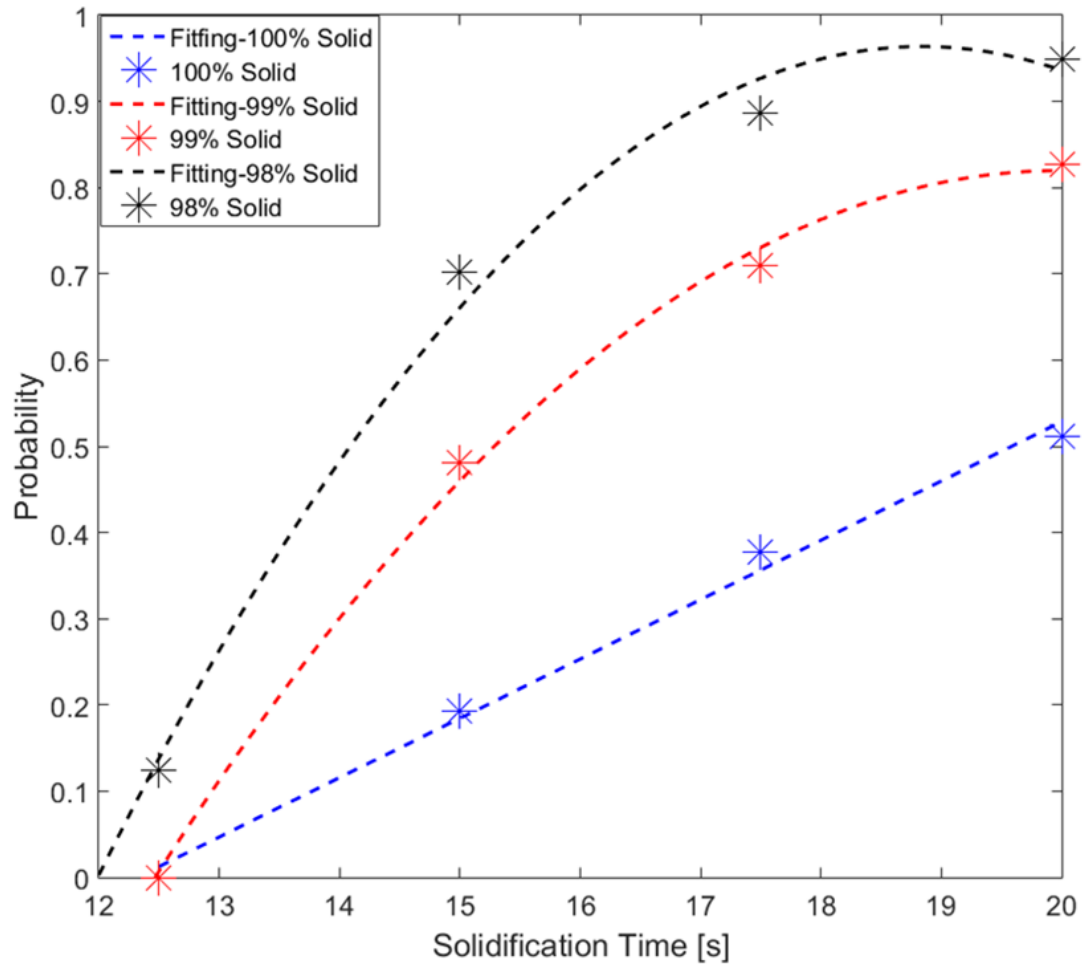
Figure 3.17. Confidence in obtaining a solid or nearly solid part as a function of solidification time. Blue points indicate the probability of obtaining 100% solid casting at multiple solidification times, red points indicate the 99% solid and black points indicate the 98% solid. Dashed lines are to guide the eye. These probability values at different solidification times are obtained by integrating the PDFs over the range of percent volume of f_s less than 1.

CHAPTER 4. UNCERTAINTY QUANTIFICATION ON SELECTED BOUNDARY CONDITIONS, SPRAYING EFFECT, AND ARTIFICIAL PARAMETERS IN HPDC

4.1   Introduction of Experiment

Based on results of both uncertainty quantification trials in Chapter 2 and 3, the IHTC representing the boundary condition of the air gap between the metal and the die has the most significant impact on the outputs of interest. However, in these two uncertainty quantification trials, only the material properties and boundary conditions with their associated uncertainty respectively are taken into consideration as inputs of interest to the PUQ analysis of the HPDC solidification model. Other operational parameters in the HPDC process, such as the intensification, spraying and blowing processes, have not yet been integrated into the uncertainty quantification. Moreover, some assumed artificial parameters required within the HPDC models, which might strongly impact the HPDC simulation results, are not yet included. Therefore, in order to quantify the effect of these other parameters on the MAGMASOFT HPDC simulation results and make a comparison with the results from previous analysis, a third uncertainty quantification investigation with well-chosen parameters, including the operational and artificial parameters, is conducted and analyzed in the following section.

4.2   Inputs of interest

In this uncertainty quantification assessment, the combined effect of the HTC of the spraying process, the feeding effectivity of casting material, and the boundary condition at the metal-die interfacial air gap are quantified.

4.2.1   Spraying Process

Spraying is an operational step during the die open period. The goal of spraying is to coat the lubricant on the surface of die cavity so that soldering damage during casting can be avoided. Considering that the lubricant actually is a mixture of a chemical and water, when sprayed toward the hot die cavity surface, it will evaporate in a short time and form a vapor layer that adversely prevents the subsequent lubricant spraying effect. This physical phenomenon is similar to two-phase boiling in natural convection. In order to help the lubricant penetrate the vapor layer, so that the chemical can cover the cavity surface efficiently, a blowing process always follows spraying. In the blowing process, an air gun blows the lubricant through the vapor layer towards the die cavity surface.

Although these operational processes do not directly affect the liquid metal solidification process, they change the initial temperature of the die cavity surface when the liquid metal is infiltrated into the cavity. The variation of initial temperature of cavity surface might have an obvious impact on the HPDC simulation results. Thus, these operational processes that might change the initial cavity surface temperature should be examined carefully. Both spraying and blowing processes are characterized by HTCs that depend on cavity surface temperature and duration of the operation. The value of the HTC for spraying is at least several times larger than that of blowing because of the

evaporation cooling during the spraying process. Therefore, in order to reduce the number of HPDC simulation cases in this uncertainty quantification, only the spraying HTC curve with uncertainty is taken into consideration as an input of interest. The spraying time for the HPDC manufacturing process of intermediate speed plate is about 6 second per cycle.

Due to lack of related experimental data for the spraying HTC curve for the real HPDC manufacturing process, the default HTC curve recommended by MAGMASOFT is used, with an assumed 30% uncertainty, as the first input of interest in this uncertainty quantification investigation. The uncertainty is assumed to obey the Gaussian distribution. The recommended HTC curve is the solid line shown in Figure 4.1, while the two dashed lines represent the uncertainty (2σ) from the Gaussian distribution. Near the peak of the curve, obvious HTC variation exists in the surface temperature range from 250 to 350 ℃. Such variation in the spraying process ultimately leads to the different initial die cavity temperatures at the time of the beginning of the filling process.
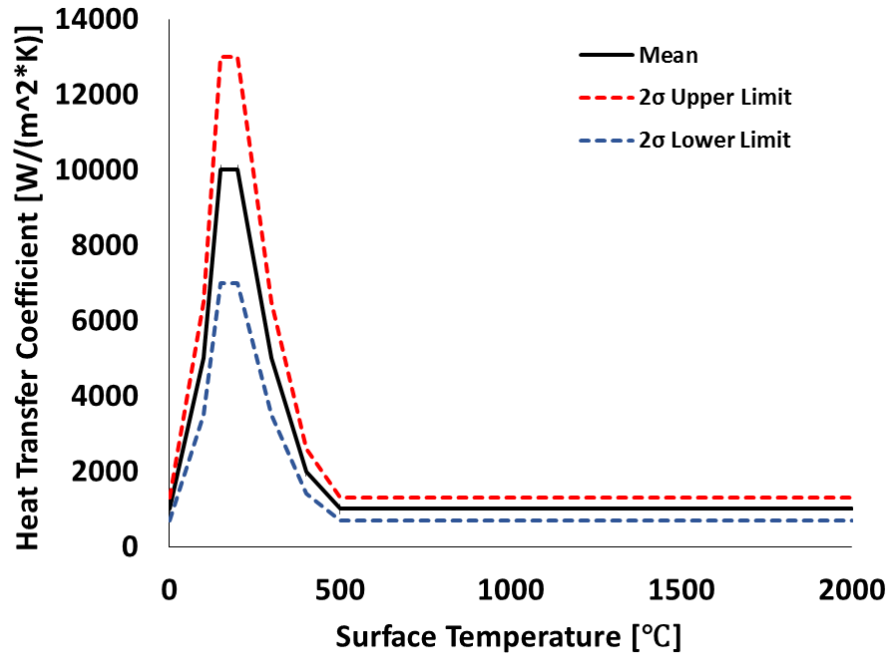
Figure 4.1. Spraying HTC as a function of die surface temperature. The black line is default spraying HTC recommended by MAGMASOFT. The two dash lines are 30% (2σ) away from default HTC (mean), representing a Gaussian distribution of uncertainty

4.2.2   Feeding Effectivity Parameter

Feeding effectivity is an artificial parameter in the model that must be defined for each

casting material. During the solidification process, each control volume can be partially

solidified and the feeding effectivity controls the flow of liquid metal into the control

volume. Specifically, the feeding effectivity defines up to which fraction solid, feeding of

the liquid metal into the control volume is possible [26]. This value has a great effect on

the formation of shrinkage pore in MAGMASOFT HPDC simulation. During the

solidification, the positions at which shrinkage pores might form are predicted by the

porosity result from MAGMASOFT. When the local fraction solid in calculated control

volume reaches the feeding effectivity value, the control volume will be cut off from the

surrounding feeding metal, representing this volume will not be included in computational domain for liquid metal transport anymore. When a large package is cut off from the feeding metal, the volume shrinkage, caused by the density difference from the liquid to the solid phase, will occur in the package as the phase transformation continues. In the end, shrinkage pores form and characterized by the volume of porosity results from MAGMASOFT. Thus, the feeding effectivity value controls the size of the potential volume in which the shrinkage pores might form.

The default feeding effectivity value recommended by MAGMASOFT is 30% which means that the computational cell will be cut off from liquid metal filling when the local fraction solid reaches 0.3. Since the feeding effectivity value is artificially assumed without any validation from experimental data, a Gaussian distribution of uncertainty, which represents confidence of precision within uncertain range, cannot be applied to describe this uncertainty distribution. Thus, a uniform distribution, in which every possible value shares the same probability density, describes the uncertainty distribution of feeding effectivity. The input feeding effectivity is assumed to be within the range from 20 to 40%.

4.2.3   Boundary Condition of Metal-die Interfacial Air Gap

Based on the uncertainty quantification results from Chapter 2 and 3, the boundary condition of air gap between metal and die has the most significant impact on the porosity and fraction liquid results from MAGMASOFT, as compared to material properties and other boundary conditions. However, the impact of this boundary condition, represented by time dependent IHTC curve discussed in Chapter 3, has not

been compared with the effect of HPDC operational processes, such as spraying, and with the effect of artificial assumed casting parameter like feeding effectivity. Therefore, the last input of interest in this uncertainty quantification investigation is the boundary condition of metal-die interfacial air gap. The IHTC curve for this boundary condition with the associated aleatoric uncertainty is the same as in Chapter 3.

<div align="center">4.3   Process of Uncertainty Quantification</div>

Three parameter in MAGMASOFT HPDC simulation—Spraying HTC curve, feeding effectivity and IHTC curve of air gap—are considered as inputs of interest in this uncertainty quantification investigation. These three inputs are submitted to the PUQ framework to obtain the required sampling cases for the MAGMASOFT HPDC simulations. The spraying HTC and air gap IHTC curves with their uncertainty are represented by Gaussian distributions, respectively in which the uncertainty is characterized by 2σ away from the mean. The uncertain feeding effectivity is represented by a uniform distribution from 20 to 40%. These three inputs are summarized in Table 4.1 and 4.2 Considering the potential interaction between inputs of interest in the HPDC process simulation, a level 2 Smolyak algorithm is applied in the sampling process. A total of 25 sampling cases are generated, each of which has its own input parameters. After finishing all simulation cases, the results of the outputs of interest are collected and submitted to PUQ framework again to obtain the surrogate model on which the following output PDFs are calculated.

Table 4.1. Input of Interest Represented by Gaussian Distribution.

Gaussian Distribution of Uncertainty		
HTC	Normalized Mean(μ)	2σ
Spraying	1	0.3μ
Interfacial air gap	1	0.3μ

Table 4.2. Input of Interest Represented by Uniform Distribution.

Uniform Distribution of Uncertainty		
Feeding Effectivity	Minimum	Maximum
	20	40

4.4   Outputs of Interest

In this uncertainty quantification trial, percent volumes of porosity and fraction liquid at

multiple solidification times are considered as the outputs of interest as previously

introduced in Chapter 2.

4.5   Results and Analysis

4.5.1   Porosity

In this uncertainty quantification investigation, the sensitivity of the predicted porosity to

the uncertain inputs of interest is shown in Figure 4.2. Spraying refers to the HTC curve

in spraying process, IHTC means the boundary condition of metal-die interfacial air gap,

and FE is the abbreviation for feeding effectivity. Based on the values of elementary

effect (represented by the height of the bars in the histogram), it is unsurprising that the

IHTC still has the greatest impact on the porosity results for the reasons preciously described in Chapter 3. The effect of spraying on the predicted porosity is so small that can be neglected. On the contrary, the effect of the uncertain feeding effectivity on the porosity is nearly half that of the IHTC boundary condition. The elementary effect value for the FE is about 0.35%, which overwhelms the effect of any other tested boundary conditions except the IHTC. This value is also larger than the elementary effect value of the tested material properties shown in Chapter 2. At the same time, the error bars in the FE histogram demonstrate that the non-linear interaction effect of feeding effectivity with IHTC boundary condition is large. Therefore, feeding effectivity becomes the second most significant parameter that determines the predicted porosity result from MAGMASOFT.

Figure 4.2. Elementary effect of spraying, boundary condition of metal-die interfacial air gap and feeding effectivity on the porosity result. The height of the histograms of *spraying, IHTC* and *FE* represent the mean (μ) of elementary effect over the uncertain range of the spraying process, boundary condition of metal-die interfacial air gap, and feeding effectivity, respectively. The error bars for each histogram indicates magnitude of the interaction on the porosity result between these inputs of interest.

The resultant PDF calculated from level 2 quadratic polynomial surrogate model for predicted porosity volume is shown in Figure 4.3. The RMSE of surrogate mode is 6.09 %, which means the surrogate model is accurate enough to replace original time-cost MAGMASOFT model for the PDF calculation. The PDF describing the model uncertainty is approximately as a Gaussian distribution with a mean (μ) of 1.3% and a deviation (σ) of 0.12%, which constitutes an uncertainty ($2\sigma/\mu$) of 18.5% for the predicted porosity. This 18.5% uncertainty in porosity determined by selected inputs of interest is larger than the 16.9% uncertainty reported in Chapter 3, which was mostly attributed to the uncertain IHTC boundary condition. Therefore, by neglecting the effect of the spraying process, the uncertain feeding effectivity contributes about 2.4% uncertainty to the porosity result from MAGMASOFT.
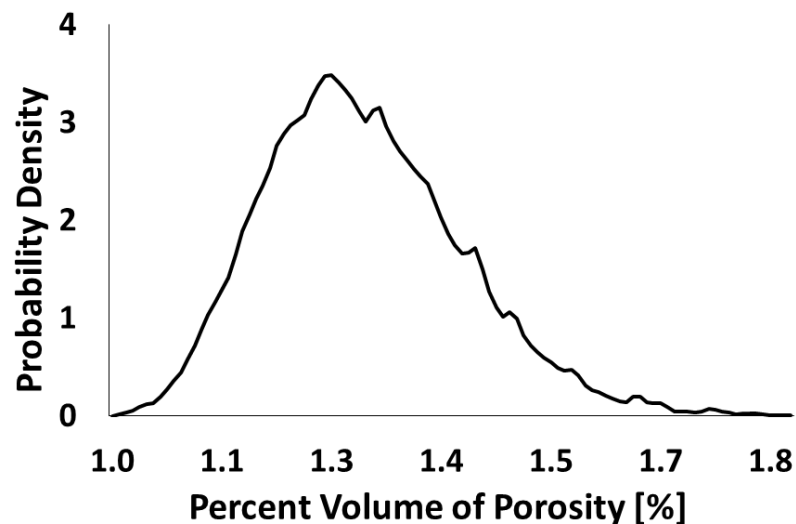
Figure 4.3. Predicted percent volume of porosity PDF with the model uncertainty propagating from the uncertain spraying effect, boundary condition of metal-die interfacial air gap, and feeding effectivity. With appropriate uncertainty in each parameters, the model predicts a distribution of predicted porosity levels: 1.3% ± 0.12%.

4.5.2   Fraction Liquid in Multiple Solidification Times

Figure 4.4 gives the sensitivity of predicted percent non-solid volume summarized by

from fraction liquid results at multiple solidification times. The mean (μ) of elementary

effect of IHTC still greatly overwhelms the effect of other two inputs of interest. The

negligible elementary effect of both feeding effectivity and spraying indicate that they

have almost no impact on the predicted fraction liquid result from MAGMASOFT. Since

the feeding effectivity value does not directly influence the local heat removal rate from

the casting, it is reasonable to conclude that it does not affect the fraction liquid result,

which is based on the solidification rate. As for the uncertain spraying HTC, although it

leads to maximum 10 ℃ variation in the initial temperature of the die cavity surface

before the filling process begins, its elementary effect on fraction liquid is also negligible.

Compared to the >600 ℃ initial liquid metal temperature before the filling process, it is

not surprising that such 10 ℃ difference in the 130°C die cavity surface does not

significantly affect the fraction liquid result. Therefore, the uncertain IHTC still controls

the variation in the fraction liquid result predicted by MAGMASOFT compared to other

inputs of interest.
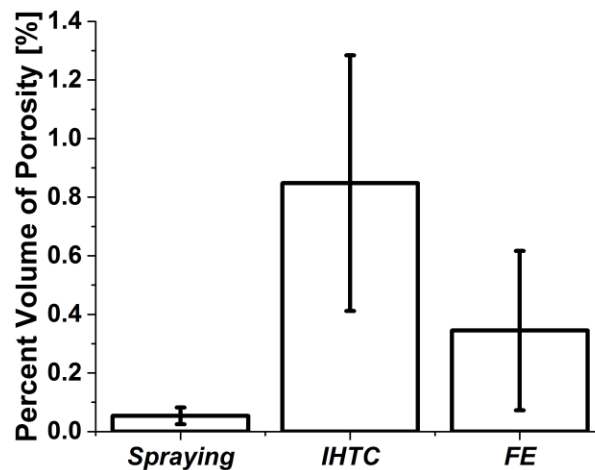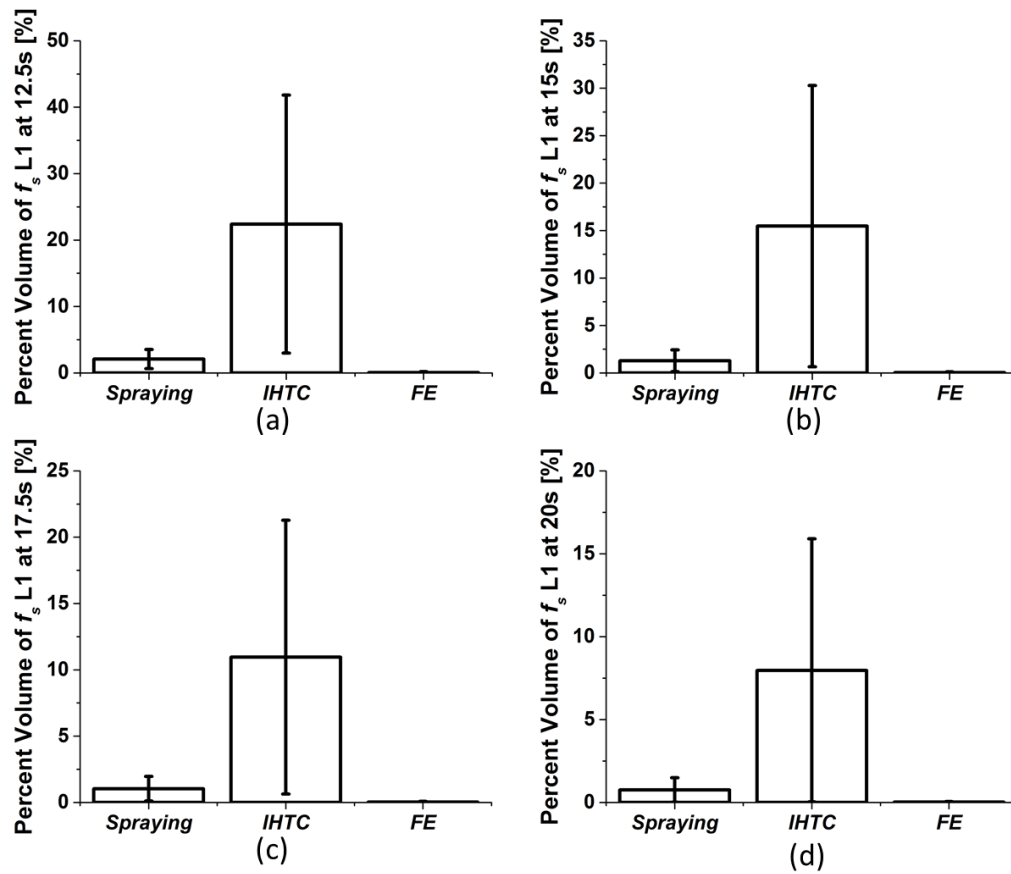
Figure 4.4. Elementary effect of spraying, boundary condition of metal-die interfacial air gap, and feeding effectivity on percent volume of fraction solid (f_s) less than 1 over the uncertain range of parameters at multiple solidification times—(a)12.5s, (b)15s, (c)17.5s and (d)20s. The height of histogram indicates the mean (μ) of elementary effect, and the error bar refers to the magnitude of interaction between input parameters.

CHAPTER 5. CONCLUSIONS

In this manuscript, the aleatoric uncertainty was quantified for an intermediate speed plate HPDC model in MAGMASOFT 5.2 with an A380 aluminum alloy as casting material. The outputs of interest included key parameters of interest related to the quality of the casting (the percent volume of porosity) and to optimizing the design of the casting process (the fraction liquid remaining at multiple solidification times). The input of interest with their uncertainty were the thermophysical properties of the material, the interfacial boundary conditions, the spraying process and the feeding effectivity (an artificial parameter used to describe the feeding of liquid metal into partially solidified zones). The results from three uncertainty quantification investigations shows that for porosity prediction, the IHTC boundary condition, representing the effect of interfacial air gap forming between casting metal and die in solidification process, needs to be known with high accuracy. The feeding effectivity value has second most significant effect on the prediction of porosity. For the prediction of the remaining fraction liquid throughout the solidification process, the same IHTC boundary condition plays the most important role. On the contrary, the impact of other input parameters on the predicted fraction liquid are negligible.

The goal of this work was to demonstrate the application of uncertainty quantification to industrial HPDC simulation. All the possible input uncertainties in this real industrial process simulation are extracted from the literature or from past work of labmates acknowledged in Chapter 3. This work sheds the light on the application of uncertainty quantification for evaluating the reliability or safety margin when designing industrial HPDC manufacturing process. The uncertainty quantification methodology demonstrated in this work can be translated to other industrial products and manufacturing processes.

LIST OF REFERENCES

LIST OF REFERENCES

[1] Diecasting.org. (2016). *FAQ*. [online] Available at:
    https://www.diecasting.org/wcm/Die_Casting/FAQ/wcm/Die_Casting/FAQ.aspx?hke
    y=01ccba73-b463-4980-b3b4-a2c28815a015 [Accessed 16 Nov. 2016].

[2] Molina, R., Amalberto, P., & Rosso, M. (2013). Mechanical characterization of
    aluminium alloys for high temperature applications Part1: Al-Si-Cu
    alloys.*Metallurgical Science and Tecnology*, *29*(1).

[3] Molina, R., Amalberto, P., & Rosso, M. (2013). Mechanical characterization of
    aluminium alloys for high temperature applications Part1: Al-Si-Cu
    alloys.*Metallurgical Science and Tecnology*, *29*(1).

[4] Swift, K. G., & Booker, J. D. (2013). *Manufacturing process selection handbook*.
    Butterworth-Heinemann.

[5] Ye, H. "An overview of the development of Al-Si-alloy based material for engine
    applications." *Journal of Materials Engineering and Performance* 12.3 (2003): 288-
    297.

[6] Dantzig, J.A., Rappaz, M. *Solidification*. EPEL Press. 2009, Print.

[7] Bergman, T. L., Incropera, F. P., DeWitt, D. P., & Lavine, A. S.
    (2011).*Fundamentals of heat and mass transfer*. John Wiley & Sons.

[8] Roy, N., Samuel, A. M., & Samuel, F. H. (1996). Porosity formation in AI-9 Wt pct
    Si-3 Wt pct Cu alloy systems: Metallographic observations.*Metallurgical and
    Materials transactions A*, *27*(2), 415-429.

[9] Wang, C. Y. & Beckermann, C. Equiaxed dendritic solidification with convection:
    Part I. Multiscale/multiphase modeling. *Metall. Mater. Trans. A* **27,** 2754–2764
    (1996).

[10] Wang, C. Y. & Beckermann, C. Equiaxed Dendritic Solidification with Convection:
    Part II. Numerical Simulations for an Al-4 Wt Pct Cu Alloy. *Metall. Mater. Trans. A*
    27, 2765–2783 (1996).

[11] Vreeman, C. J. & Incropera, F. P. Numerical Discretization of Species Equation Source Terms in Binary Mixture Models of Solidification and Their Impact on Macrosegregation in Semicontinuous, Direct Chill Casting Systems. *Numer. Heat Transf. Part B Fundam.* **36,** 1–14 (1999).

[12] Vreeman, C. J., Krane, M. J. M. & Incropera, F. P. The effect of free-floating dendrites and convection on macrosegregation in direct chill cast aluminum alloys Part I : model development. *Int. J. Heat Mass Transf.* **43,** 677–686 (2000).

[13] Vreeman, C. J. & Incropera, F. P. The effect of free-floating dendrites and convection on macrosegregation in direct chill cast aluminum alloys Part II : predictions for Al ± Cu and Al ± Mg alloys. *Int. J. Heat Mass Transf.* **43,** 687–704 (2000).

[14] Fezi, K., Plotkowski, A. & Krane, M. J. M. Macrosegregation Modeling During Direct Chill Casting of Aluminum Alloy 7050. *Numer. Heat Transf. Part A Appl.* (in review).

[15] Fezi, K. and Krane, M. J. M. Uncertainty Quantification in Modeling Metal Alloy Solidification. *Journal of Heat Transfer.* (in review).

[16] Fezi, K. and Krane, M. J. M. Uncertainty Quantification in Modeling Equiaxed Alloy Solidification. *International Journal of Cast Metals Research.* (Accepted).

[17] Chernatynskiy, A., Phillpot, S. R., & LeSar, R. (2013). Uncertainty quantification in multiscale simulation of materials: A prospective. *Annual Review of Materials Research*, *43*, 157-182.

[18] Kumar, A., Založnik, M., & Combeau, H. (2012). Study of the influence of mushy zone permeability laws on macro-and meso-segregations predictions.*International Journal of Thermal Sciences*, *54*, 33-47.

[19] Fezi, K., & Krane, M. J. M. (2015). Uncertainty Quantification in Solidification Modelling. In *IOP Conference Series: Materials Science and Engineering* (Vol. 84, No. 1, p. 012001). IOP Publishing.

[20] Fishman, G. (2013). *Monte Carlo: concepts, algorithms, and applications*. Springer Science & Business Media.

[21] Koslowski, M., & Strachan, A. (2011). Uncertainty propagation in a multiscale model of nanocrystalline plasticity. *Reliability Engineering & System Safety*, *96*(9), 1161-1170.

[22] Hunt, M, et al. "PUQ: A code for non-intrusive uncertainty propagation in computer simulations." *Computer Physics Communications* 194 (2015): 97-107.

[23] Smolyak, S. A. "Quadrature and interpolation formulas for tensor products of certain classes of functions." *Dokl. Akad. Nauk SSSR*. Vol. 4. No. 240-243. 1963.

[24] Eldred, M. S. (2009). Recent advances in non-intrusive polynomial chaos and stochastic collocation methods for uncertainty analysis and design.*AIAA Paper*, *2274*(2009), 37.

[25] Campolongo, F., Cariboni, J., & Saltelli, A. (2007). An effective screening design for sensitivity analysis of large models. *Environmental modelling & software*, *22*(10), 1509-1518.

[26] MAGMASOFT v5.2, MAGMA GmbH, Aachen, Germany.

[27] Fezi, K. and Krane, M. J. M. Uncertainty Propergation in Numerical Modeling of Aluminum Direct Chill Casting. *Metall. Mater Trans B.* (Submitted).

[28] Fezi, K., Plotkowski, A., & Krane, M. J. (2016). A Metric for the Quantification of Macrosegregation During Alloy Solidification. *Metallurgical and Materials Transactions A*, *47*(6), 2940-2951.

[29] Brandt, R., & Neuer, G. (2007). Electrical resistivity and thermal conductivity of pure aluminum and aluminum alloys up to and above the melting temperature. *International Journal of Thermophysics*, *28*(5), 1429-1446.

[30] Overfelt, R. A., Bakhtiyarov, S. I., & Taylor, R. E. (2002). Thermophysical properties of A201, A319, and A356 aluminium casting alloys. *High Temperatures-High Pressures*, *34*(4), 401-410.

[31] Rudtsch, S. "Uncertainty of heat capacity measurements with differential scanning calorimeters." *Thermochimica Acta* 382.1 (2002): 17-25.

[32] Morrell, R., & Quested, P. (2004). Evaluation of piston dilatometry for studying the melting behaviour of metals and alloys. *HIGH TEMPERATURES HIGH PRESSURES*, *35*(4), 417.

[33] Đurđević, M. B., et al. "Modeling of casting processes parameters for the 3xx series of aluminum alloys using the silicon equivalency algorithm."*Metalurgija* 9.2 (2003): 91-106.

[34] Djurdjevic, M. B., et al. "Comparison of different analytical methods for the calculation of latent heat of solidification of 3XX aluminum alloys." *Materials Science and Engineering: A* 386.1 (2004): 277-283.

[35] Winterton, R. H. S. "Where did the Dittus and Boelter equation come from?."*International Journal of Heat and Mass Transfer* 41.4 (1998): 809-810.

[36] Jo, D, et al. "Experimental investigation of convective heat transfer in a narrow rectangular channel for upward and downward flows." *Nuclear Engineering and Technology* 46.2 (2014): 195-206.

[37] Taler, J., & Zima, W. (1999). Solution of inverse heat conduction problems using control volume approach. *International Journal of Heat and Mass Transfer*, *42*(6), 1123-1140.

[38] Plotkowski, A., & Krane, M. J. M. (2015). The Use of Inverse Heat Conduction Models for Estimation of Transient Surface Heat Flux in Electroslag Remelting. *Journal of Heat Transfer*, *137*(3), 031301.

[39] Beck, J. V. "Nonlinear estimation applied to the nonlinear inverse heat conduction problem." *International Journal of heat and mass transfer* 13.4 (1970): 703-716.

[40] Beck, J. V., Litkouhi, B., & Clair Jr, C. S. (1982). Efficient sequential solution of the nonlinear inverse heat conduction problem. *Numerical Heat Transfer, Part A Applications*, *5*(3), 275-286.

[41] Beck, J. V., Blackwell, B., & Haji-Sheikh, A. (1996). Comparison of some inverse heat conduction methods using experimental data. *International Journal of Heat and Mass Transfer*, *39*(17), 3649-3657.

[42] Chen, L., Wang, Y., Peng, L., Fu, P., & Jiang, H. (2014). Study on the interfacial heat transfer coefficient between AZ91D magnesium alloy and silica sand. *Experimental Thermal and Fluid Science*, *54*, 196-203.

[43] Sun, Z., Hu, H., & Niu, X. (2011). Determination of heat transfer coefficients by extrapolation and numerical inverse methods in squeeze casting of magnesium alloy AM60. *Journal of Materials Processing Technology*, *211*(8), 1432-1440.

[44] Guo, Z. P., Xiong, S. M., Liu, B. C., Li, M., & Allison, J. (2008). Effect of process parameters, casting thickness, and alloys on the interfacial heat-transfer coefficient in the high-pressure die-casting process. *Metallurgical and Materials Transactions A*, *39*(12), 2896-2905.

[45] Guo, Z. P., Xiong, S. M., Liu, B. C., Li, M., & Allison, J. (2008). Determination of the heat transfer coefficient at metal–die interface of high pressure die casting process of am50 alloy. *International journal of heat and mass transfer*, *51*(25), 6032-6038.

[46] Cao, Y., Guo, Z., & Xiong, S. (2012). Determination of the metal/die interfacial heat transfer coefficient of high pressure die cast B390 alloy. In *IOP Conference Series: Materials Science and Engineering* (Vol. 33, No. 1, p. 012010). IOP Publishing.

[47] Dargusch, M. S., Hamasaiid, A., Dour, G., Loulou, T., Davidson, C. J., & StJohn, D. H. (2007). The Accurate Determination of Heat Transfer Coefficient and its Evolution with Time During High Pressure Die Casting of Al‑9% Si‑3% Cu and Mg‑9% Al‑1% Zn Alloys. *Advanced Engineering Materials*, *9*(11), 995-999.

[48] Dour, G., Dargusch, M., Davidson, C., & Nef, A. (2005). Development of a non-intrusive heat transfer coefficient gauge and its application to high pressure die casting: effect of the process parameters. *Journal of Materials Processing Technology*, *169*(2), 223-233.

APPENDIX

APPENDIX

The error of surrogate models for all three uncertainty quantification investigations are

shown in the following tables. Root Mean Square Error (RMSE) and Normalized Root

Mean Square Error (NRMSE) are used as the parameters to determine whether the

surrogate models are accurate enough to replace the original numerical model in

MAGMASOFT in the uncertainty quantification investigations. The RMSE and NRMSE

for each surrogate models are calculated based on:

$$\text{RMSE} = \sqrt{\frac{\sum_{t=1}^{n}(\hat{y}_t - y_t)^2}{n}} \tag{10}$$

and

$$\text{NRMSE} = \frac{RMSE}{y_{max} - y_{min}} \tag{11}$$

where $\hat{y}_t$ is the output calculated from the surrogate model, y_t is the output from the

MAGMASOFT HPDC simulation and *n* is the simulations number. In addition to the

necessary simulations required in PUQ, extra simulations with randomly input

parameters are finished and their output results are integrated in the RMSE and NRMSE

calculation. If the NRMSE is small enough, the accuracy of surrogate model is sufficient

to replace the complex numerical model of MAGMASOFT. If the NRMSE values for

both "with & without extra

simulations" groups are close, the surrogate model is verified to be accurate to predict the outputs with other input parameters.

The results in the three tables below show that the NRMSD of the surrogate models of the porosity volume and fraction liquid at multiple solidification times remains in a low level. This means the calculated results from these surrogate models are not significantly different from the results from MAGMASOFT HPDC simulations. Moreover, the NRMSD values for both "with & without extra simulations" groups are very close. That means with other input parameters, the surrogate models also generate accurate enough results compared with the ones from the MAGMASOFT simulations. Thus, the small NRMSD values prove that the surrogate models of the porosity volume and fraction liquid at multiple solidification times can be applied in the uncertainty quantification.

However, the NRMSD of the surrogate models of the hot spot (three hot spots are indicated in Fig. A.1) is quite large. That means these surrogate models of the hot spots are not accurate enough to approximate the numerical model of MAGMASOFT. Thus, these surrogate models should be abandoned and no level 2 uncertainty quantification on hot spots was done in this study. In order to evaluation the uncertainty of the hot spot results, a higher level of the smolyak algorithm needs to be selected to generate a higher order of the polynomial surrogate model for the reduced NRMSD value.
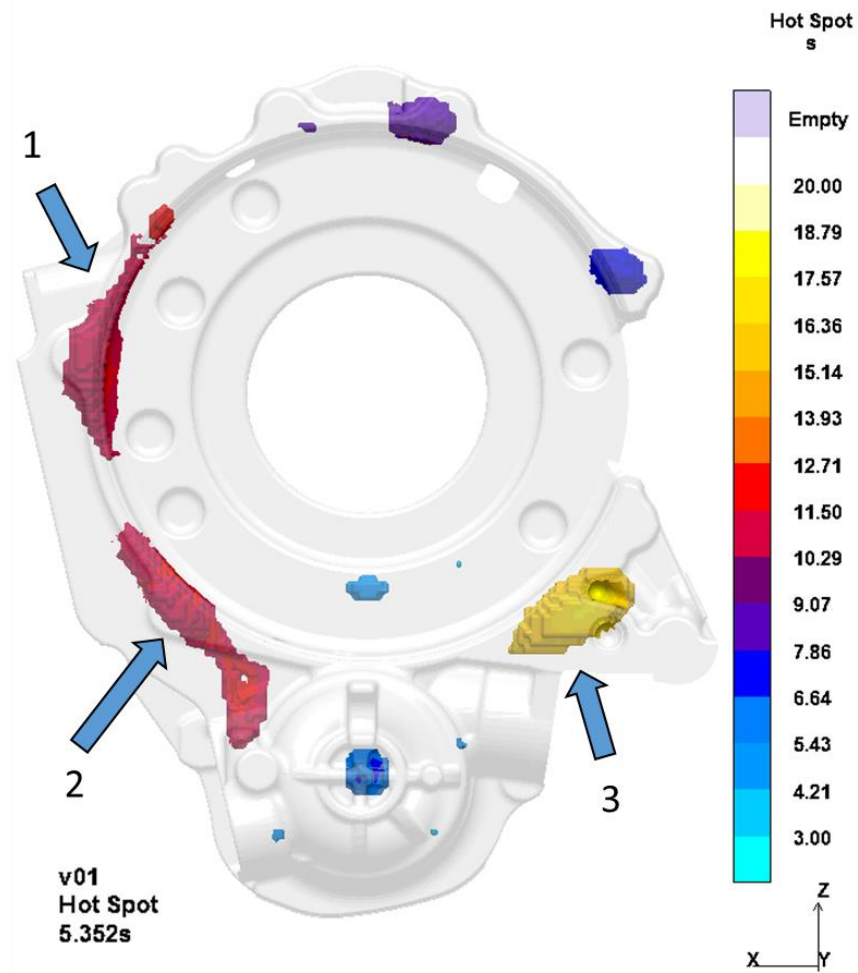
Figure A.1. Selected Hot Spot #1, #2 and #3 for intended uncertainty quantification. The volume of the each three hot spots are collected and submitted to PUQ to generate the surrogate model. Different Colors shows when each hot spot forms during the solidification process.

Table A.1. Surrogate Model Accuracy Evaluation for UQ on Casting Material Thermophysical Properties.

Surrogate model	Without Extra Simulations		With Extra Simulations	
	RMSD (cm³)	NRMSD (%)	RMSD (cm³)	NRMSD (%)
Porosity Volume	0.2363	15.0496	0.2037	12.9759
Fraction Liquid 12.5s	0.2983	1.0822	0.2881	1.0452
Fraction Liquid 15s	0.1557	1.0360	0.1488	0.9902
Fraction Liquid 17.5s	0.1935	2.5669	0.1774	2.3523
Fraction Liquid 20s	0.2761	14.4544	0.2593	13.5770
Hot_Spot_1	6.2598	61.5515	5.5144	54.2225
Hot_Spot_2	7.0648	57.9559	6.6608	54.6418
Hot_Spot_3	0.7914	26.9176	0.7387	25.1243

Table A.2. Surrogate Model Accuracy Evaluation for UQ on Boundary Conditions on HPDC.

Surrogate model	Without Extra Simulations		With Extra Simulations	
	RMSD (cm³)	NRMSD (%)	RMSD (cm³)	NRMSD (%)
Porosity Volume	0.2378	3.9184	0.2203	3.6292
Fraction Liquid 12.5s	11.5451	7.5925	10.3668	6.8176
Fraction Liquid 15s	14.0963	13.8212	12.2667	12.0274
Fraction Liquid 17.5s	9.7452	13.4770	8.4292	11.6570
Fraction Liquid 20s	5.2946	10.0506	4.6183	8.7667
Hot_Spot_1	2.2977	48.3721	2.0874	42.6863
Hot_Spot_2	3.8397	52.9613	3.6228	49.9697
Hot_Spot_3	NA	NA	NA	NA

Table A.3. Surrogate Model Accuracy Evaluation for UQ on Selected Boundary
Conditions, Spraying Effect and Feeding Effectivity on HPDC.

Surrogate Model	Without Extra Simulations		With Extra Simulations	
	RMSD (cm³)	NRMSD (%)	RMSD (cm³)	NRMSD (%)
Porosity Volume	0.5461	6.0885	0.5220	5.8199
Fraction Liquid 12.5s	11.5548	6.8166	10.9904	6.4837
Fraction Liquid 15s	13.6862	11.5339	12.8537	10.8324
Fraction Liquid 17.5s	9.4985	11.1198	8.8905	10.4080
Fraction Liquid 20s	5.3317	8.5526	5.0124	8.0403
Hot_Spot_1	2.0662	33.1114	1.9663	31.5110
Hot_Spot_2	3.4531	53.4542	3.4165	49.2995
Hot_Spot_3	NA	NA	NA	NA